ISSN 1843 - 7583

Carpathian Journal of Electrical Engineering Volume 6, Number 1, 2012

Volume 6, Number 1, 2012

Technical University of Cluj-Napoca
North University Centre of Baia Mare
Faculty of Engineering
Electrical. Electronic and Computer Engineering Department

Carpathian Journal of Electrical Engineering

NORDTECH PUBLISHER

TECHNICAL UNIVERSITY
OF CLUJ-NAPOCA

NORTH UNIVERSITY CENTRE OF BAIA MARE
ENGINEERING FACULTY

ELECTRICAL, ELECTRONIC AND
COMPUTER ENGINEERING DEPARTMENT

Carpathian Journal of Electrical Engineering

Volume 6, Number 1, 2012
ISSN 1843 – 7583

http://cee.ubm.ro/cjee.html

CONTENTS

STUDY OF ELECTRIC CAPACITORS USING FINITE ELEMENT METHOD

Alina **NEAMȚ**, Anca **BĂRCUTEANU**
Technical College Anghel Saligny Baia Mare
alina23_tatiana @yahoo.com, ancasiminabarcuteanu@yahoo.com

Key words: plane capacitor, dielectric, rigidity, permittivity, capacitance, Finite Element Method

Abstract: *A capacitor is made of two armatures and a dielectric between the two armatures. In this paper, we are going to study the plane capacitor , which is made of two equal metal armatures, plane and parallel, having the S surface, situated at a distance d much shorter than the armatures dimensions, between which there is a liniar, homogenous and isotropic dielectric having a constant electrical permittivity.The purpose of studying the plane capacitor, through MEF, presented in this paper,is to establish the stress to which the dielectrics may be subject to, in daily practice, and the influence that their superposition in an electric field has, on each of them. The study of the plane capacitor , finalised with observations on the raise of the dependence of the electric field intensity in air on the size of the air layer and having as parameter the type of dielectric material introduced between the armatures, is an example of confirmation or invalidation of the possibility and utility of using layers of dielectrics between the armatures of the capacitors.*

1. THE PLANE CAPACITOR

1.1 General concepts

It is taken into consideration a system made of two conductors *1, 2* loaded with equal, real electrical charges which are opposite and situated into a dielectric medium that can be either isotropical or unisotropical, liniar or unaligned, homogenous or inhomogenous, but electrically uncharged and without permanent polarisation. The capacitor is such a device (*see fig.1*). The two metallical conductors of the system are called the armatures of the capacitor. The form and the layout of these may vary.

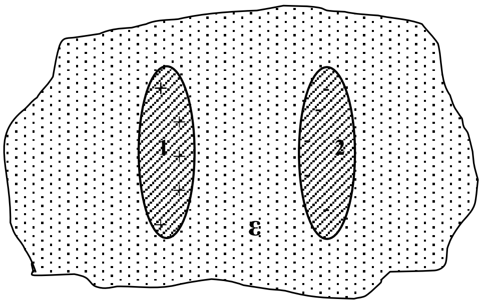

Figure 1. Capacitor

The imposed condition that the electrical charges of the armatures should be equal and of opposite value shows the fact that we are dealing with a complete electrical field, which means that all the field lines starting on one armature end on the other one. The proportion between the electrical charge of one of the conductors and the difference of potential, respectively the voltage between one conductor and the other is a positive value C, called *electrical capacitance of the capacitor*:

$$C = \frac{Q_1}{V_1 - V_2} = \frac{Q_1}{U_{12}} > 0 \tag{1}$$

or

$$C = \frac{Q_2}{V_2 - V_1} = \frac{Q_2}{U_{21}} > 0 \tag{2}$$

Since $Q_2 = -Q_1$, and $V_1 - V_2 = -(V_2 - V_1)$. The reciprocal value $S = 1/C$ is also called elastic capacitance of the capacitor.

If the dielectrical value between the armatures is liniar, according to the theory of the superposition, the charge on the armature varies directly proportionally with the potentials, that is with the difference of potential between the armatures.Therefore, the electrical capacitance in this situation is independent from the electrical charge, that is from the difference of potential, being a characteristic value of the respective capacitor.

In the case of the unaligned dielectricals, the electrical charge not being proportional with the difference of potential, the capacitance is not a constant one. In this case, the capacitance defined by the relation (*1*) is also called static capacitance.

Related to the above mentioned concepts, there are some specifications to be made:

- Electrical capacitance is a global parameter of a capacitor, based on a defining ratio. Nevertheless, the term „capacitance" should not be used, as it often happens, to define the technical device itself; for this, one should use the term „capacitor".

- The capacitance of a condenser depends on the geometry and the dimensions of the armatures system and also on the nature of the dielectric between the armatures.

- The defining equation of capacitance may also be applied, by principle, in a varied system.In general, up until high voltages, we may consider the values of capacitance established in an electrostatic system.These values must be changed, though, if in the dielectric between the armatures appears, for example, the post effect. It may also be mentioned the fact that capacitance is not the only parameter of a capacitor, in general. Thus, due to the finite conductivity of the real dielectrics and in the case of high voltages due to the supplementary losses , the capacitor is also defined by a certain resistance.

- To the capacitors used for practical training, one must also indicate the working tension, besides the capacitance; this should be stated because if the tension in the capacitor outgrades a certain value, the dielectric between the armatures will pe pierced.

- The term of capacitance is inherent not only to capacitors , but also in the case of other technical systems. In this case we may spekak of, for example, the capacitance between turns, the capacitance of an electrical line, the capacitance between the electrolytes of an electronic tube etc.; in all of these situations, we may speak of an electric field occurring, having a certain configuration and having a correspondent capacitance.

Classification of capacitors:

- *According to their type of dielectrics*, there are: the gasous dielectric capacitors(vacuum, air, gas); liquid (oil); solid anorganic (glass, enamel, ceramics); solid organic (paper, polish, synthetical enamel); metal oxydes (electrolitical).
- *According to their construction design*, we have: still, variable, semi-adjustable (adjustable).
- *According to their working system*, there are capacitors for: continuous current, alternative current, high voltages.
- *According to their working tension*, capacitors may be: low tension, high tension.
- *According to their material* we may distinguish: capacitors in plastic shell; in metal shell, in ceramics shell.

1.2. Elements of technology

Still capacitors with air are made of several metal plates, which are parallel and distanced. The plates form two groups, insulated by ceramical supports. These are made of silvered brass or aluminium and they form the armatures of the capacitor.

Variable capacitors with air are generally made of mobile plaquettes of aluminiun thin sheets obtained through punching, called the rotor, which are introduced by rotating movements between the still thin sheets, called the stator.

Capacitors made of mica are formed of thin metal sheets applied by pressure on the surface of the insulating material or by spraying a thin layer on the surface of the mica plate. The impregnation of the capacitor is made in mineral wax, epoxy resin, etc.

Ceramics capacitors shaped as a disk, a plaquette, a pan or tubular ones, have the dielectric made of ceramics plaquettes obtained from steatite or magnesium titanate. The electrodes are made by silvering the two facettes of the dielectric; the protection of the capacitor is made of wax, epoxy resin, plastic, etc.

Paper capacitors are made of aluminium thin sheets in which are introduced layers of special paper, that is impregnated with wax or mineral oil. The technical procedures are: the positionning of the aluminium and paper layers; the rolling of the layers as a cylindrical roll or as a flat cylinder; impregnating the paper with oil, resin or mineral wax.

Electrolyte capacitors are based on the chemical reaction between an electrolyte and a metal, which forms a layer of insulating oxide that makes the dielectric.

Electrolyte capacitors with electrolyte liquid are made of an aliminium tube in which are put the anode from oxidised aluminium and the liquid electrolyte obtained from a boracic acid solution .

Semidry electrolyte capacitors are obtained from the simultaneous rolling of the following elements: oxidised aluminium foil, forming the anode , paper band, a second aluminium foil , forming the cathode.

The resulting roll is impregnated in boracic acid solution, ethylene glycol and ammonium hydroxide. The procedure is to be made under vacuum conditions.Because the oxide film gets deteriorated during the rolling and impregnation technologies, it has to be restored by applying a tension which is raised , gradually, above 0 , for a few hours; the same procedure is to be made if the capacitor has not been used for about one year.

The most often used capacitors are the ones with sintered anodes.The anode is made of a body of synthesised tantalum powder.

Sintered anodes are oxidised and then impregnated with an electrolyte formed of phosphoric and sulphuric acid combined with lithium chloride , while the cathode is a silver capsule.

Capacitors are used in: radiotechnics, television, radiolocation, telephony and telegraphy , for improving the functioning parameters in networks, fluorescent lamps, transformers and to start monophasic engines.

Industrial capacitors have the dielectric under relatively heavy loads, because of its functioning at high voltage and industrial frequency. The dielectric losses also stress the insulation, causing the heating of the capacitor.

In the dielectric, it is generally used paper made of different fabrics.As impregnating liquid, mineral oil or chlorinated oil are used. There is also the option of using alternative paper and plastic film layers in the dielectric, in which case we are talking about the mixed dielectric.

The„all film"capacitors have as solid insulation material several layers of plastic film and are contructed similarly to the paper/oil capacitors..

The MP capacitors have their armature metalised by evaporation, in vacuum, directly on the paper support.

The MKV capacitors also have their armature metalised by evaporation, in vacuum, but on both sides of the paper, which only has the role of impregnation wick. The dielectric is made of a layer of polypropylene film.

The MKP capacitors have the armature metalised by evaporation, in vacuum, directly on a plastic support. They are built dry or are filled with an electronegative gas.

1.3. The plane capacitor

The plane capacitor is made of two equal metal armatures, plane and parallel, having the S surface, situated at a distance *d* much shorter than the armatures dimensions, between which there is a liniar, homogenous and isotropic dielectric having a constant electrical permittivity *fig.2*. The thickness of the armatures is considered to be negligible.

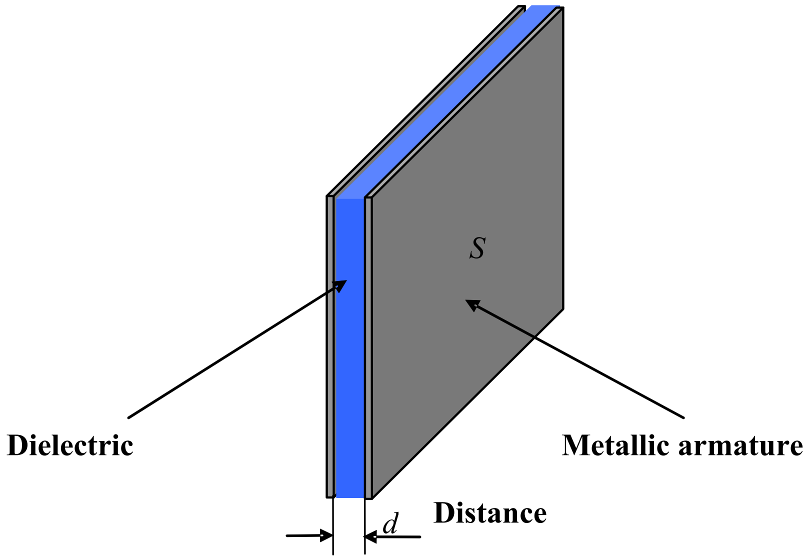

Figure 2. The plane capacitor

Obviously, the configurations obtained by replacing the homogenous, liniar isotropic dielectric by another one (nin liniar, non homogenous ,etc.) are also called plane capacitors. Such cases will be analysed and interpreted in the present paper by taking into account the electrical stress on the dielectric.

1.4. How to calculate the electrical charge, the intensity of the electric field and the capacitance of the plane capacitor

Faraday's law, particularised for the electrostatic condition and Gauss's law, together with the constitutive equation lead to the Laplace equation, which represents the starting point in the MEF analysis of the plane capacitor –type configurations.

Gauss's law allows, in its integral form, the identification of the electric charge of an armature:

$$\int_{\Sigma} \overline{D} \cdot \overline{ds} = Q \qquad (3)$$

The closed surface Σ surrounds one of the capacitor's armatures, the surface $\overline{ds}$ being considered based on the exterior normal.

The MEF post processing of the meshed potential values set, generated by a first order triangle elements meshing, leads to a single value of the electric field intensity, that is a single value for the electrical induction in each element. This aspect implies an attentive meshing of the domein to analyse , to offer all along the Σ surface sufficient values for these measurements , on one hand, and a correlation of the number of elements with the variations of the field in certain areas, on the other hand.

Calculating the capacitance becomes an easy task, using the (1) equation, after calculating the electric charge.

The analytical way of calculating , while taking into consideration the uniform field between the armatures and by neglecting the edge effect, becomes, obviously, very simple:

$$V_1 - V_2 = U_{12} = \int_1^2 \overline{E} \cdot \overline{dl} = \frac{\rho_S \cdot d}{\varepsilon} = \frac{Q \cdot d}{\varepsilon \cdot S} \tag{4}$$

in which the line integral is calculated between the armatures *1* and *2* , resulting:

$$E = \frac{V_1 - V_2}{d} \tag{5}$$

By using (1) and (4) one may determine the capacitance of the plain capacitor with a uniform field:

$$C = \frac{\varepsilon \cdot S}{d} \tag{6}$$

Making these measurements is equally easy in the case of liniar, isotropical and homogenous dielectrics, placed in parallel layers between the armatures, but still considering a uniform electrical field.Thus, we consider a dielectric formed of two layers, parallel to the armatures, which have d_1 and d_2 thickness values, and ε_1 and ε_2 permittivity values *:*

By expressing the difference of potential between the armatures, we get:

$$V_1 - V_2 = U_{12} = \int_1^2 \overline{E} \cdot \overline{dl} = E_1 \cdot d_1 + E_2 \cdot d_2 = \frac{Q}{S} \cdot \left(\frac{d_1}{\varepsilon_1} + \frac{d_2}{\varepsilon_2} \right) \tag{7}$$

resulting the capacitance of the plain capacitor with a non-homogenous, two-layered dielectric:

$$C = \frac{S}{\dfrac{d_1}{\varepsilon_1} + \dfrac{d_2}{\varepsilon_2}} \tag{8}$$

Taking into consideration the interface condition between two dielectrics on which the charge density is zero and the constitutive equation, we may conclude:

$$\frac{E_{1n}}{E_{2n}} = \frac{\varepsilon_2}{\varepsilon_1} \tag{9}$$

In the analysed configuration, there are only normal components of the intensity of the electrical field and from (7) and (8), the expressions of this item in the two dielectric

$$E_1 = \frac{V_1 - V_2}{d_1 + \frac{\varepsilon_1}{\varepsilon_2} \cdot d_2} \tag{10}$$

and

$$E_2 = \frac{V_1 - V_2}{d_2 + \frac{\varepsilon_2}{\varepsilon_1} \cdot d_1} \tag{11}$$

The calculus of these items , should we consider the edge effect, is a problem without an analytical solution, the calculation methods involved being numerical ones. In all the configurations analysed through MEF , analytical solutions will be given in this paper, in order to estimate the influence of not taking into consideration the edge effect.

1.5. The study, through MEF, of the plane capacitor with a liniar, isotropic and homogenous dielectric

The configurations to be studied include the plane capacitor with a liniar, isotropic and homogenous dielectric, having a relative permittivity ε_r ,with the armatures in a square shape with *16 mm* long side, the distance between the armatures being *4 mm*, connected to *8 KV* difference of potential and a parallelepiped cutting through the domain situated at *16 mm* distance all around the capacitor , on the surface of which are defined homogenous Neuman-type bordering conditions. The size of the parallelepiped has been chosen, after numerous trials, in such a way that the infinite border condition should not be affected by significant errors and the study field should not be too vast – a thing that would require a very large amount of elements.

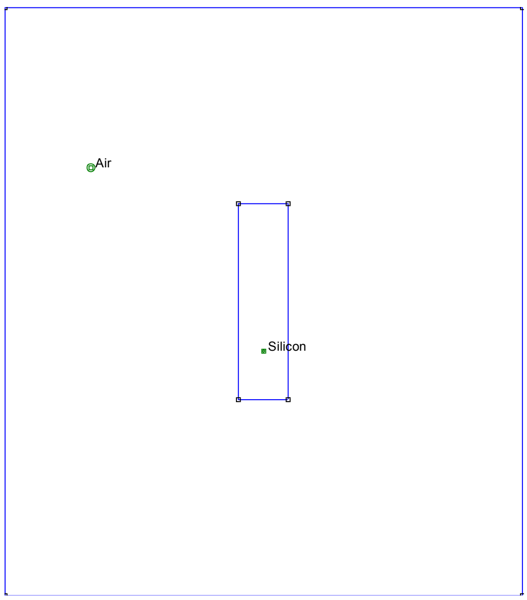

Figure 3.The plane-parallel analysed configuration, having silicone as dielectric

The MEF analyses have been made using the same device as in the case of the FEMM 4.0 electromagnet, a fact which imposed the 2D analysis. This led to transferring the tridimensional problem to a plane parallel one.

We have put under study the capacitors having the following dielectric: air, $\varepsilon_r = 1$; rubber, $\varepsilon_r = 3$; mica, $\varepsilon_r = 6$ and silicone $\varepsilon_r = 12$. The four configurations are geometrically identical, only the dielectric type being different, *Fig.3 for the silicone dielectric*.

The meshing of the field, offered automatically by the programme, is not satisfactory not even for showing the equipotential lines, much less for the calculation and the phenomenological interpretation of certain values. Bearing in mind the things revealed by the calculus of the electric charge (paragraph III 2.4), the meshing network will be refined like this: the accentuated thickening in the capacitor dielectric, setting a smaller size for the sides of the elements forming the armatures and for the dielectric-air separation area, in order to create an area with a greater number of elements on the line of the integration curve of the normal component belonging to the electric induction.

The accordingly refined meshing , *Fig. 4*, includes 15507 nodes and 30646 elements.

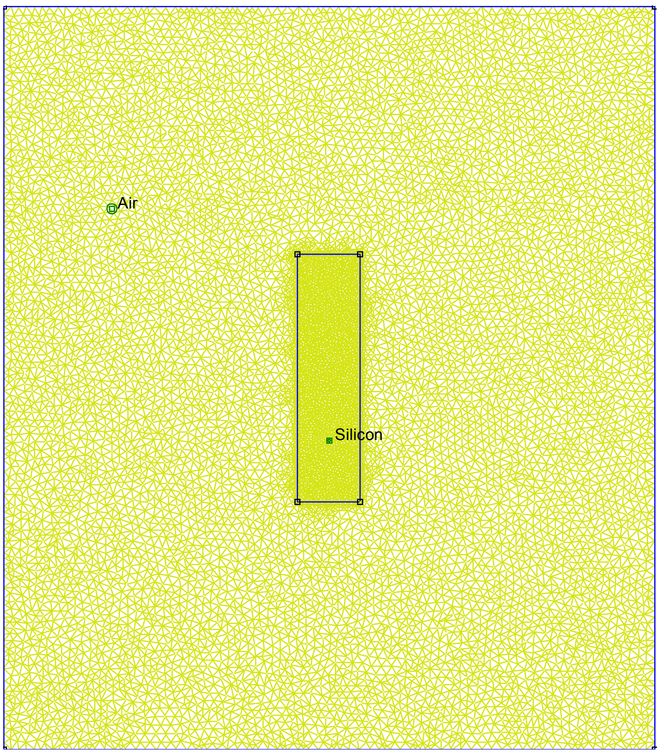

Figure 4. Refined meshing

Starting with this network, the MEF analysis offers the values of the electrical potential in any point of the field. Based on these facts, it is easy to figure out the aspect of the equipotential lines, *fig. 5,* an example for the silicone dielectric.

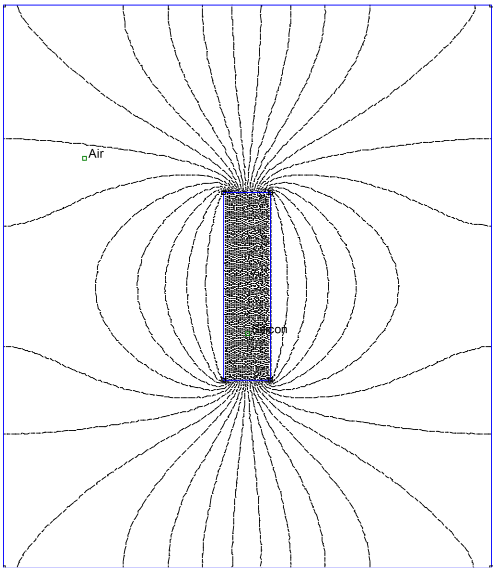

Figure 5. The equipotential lines for the dielectric, silicone

It is also the solutions found for potential that allow us to calculate the intensity of the electric field and the electrical induction. The device used for doing this, FEMM 4.0, allows the mapping out the distribution of the electric field intensity, *Fig. 6,* for silicone.

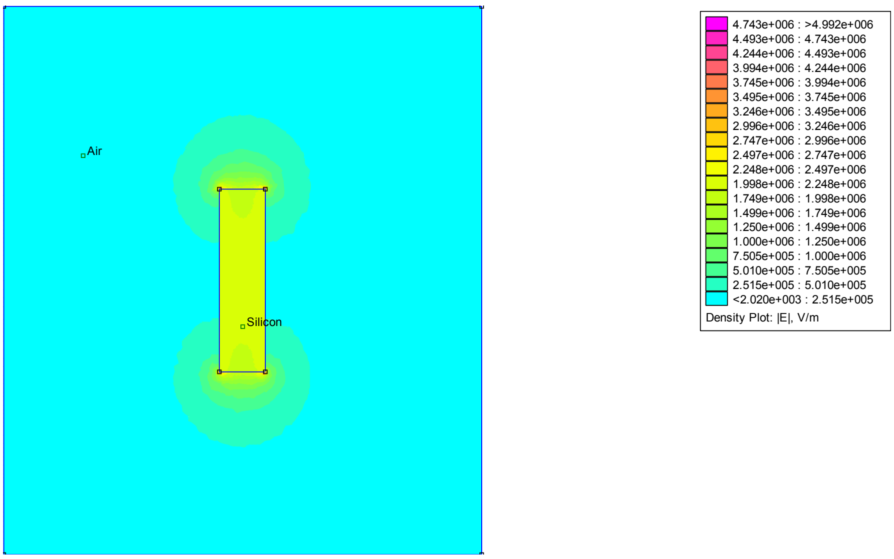

Figure 6. The distribution of the electric field intensity in the case of silicone as dielectric material, between the armatures

Very useful and explicit, besides the equipotential lines map, in visualising the influence of the edge effect on the plane capacitor, is also the distribution of the electrical intensity within a central section, between the armatures , which is parallel to these, *figure 7*. One may notice the decreasing of this value near the edges of the capacitor, a decreasing which becomes more accentuated with the decreasing of the relative permittivity of the dielectric. Thus, the values on the dielectric-air separation surface decrease from *19,4 KV/cm*, in the case of the silicone, to *17,9 KV/cm*, when using the rubber as dielectric and reaching

15,8 KV/cm in the case of the air-air separation.

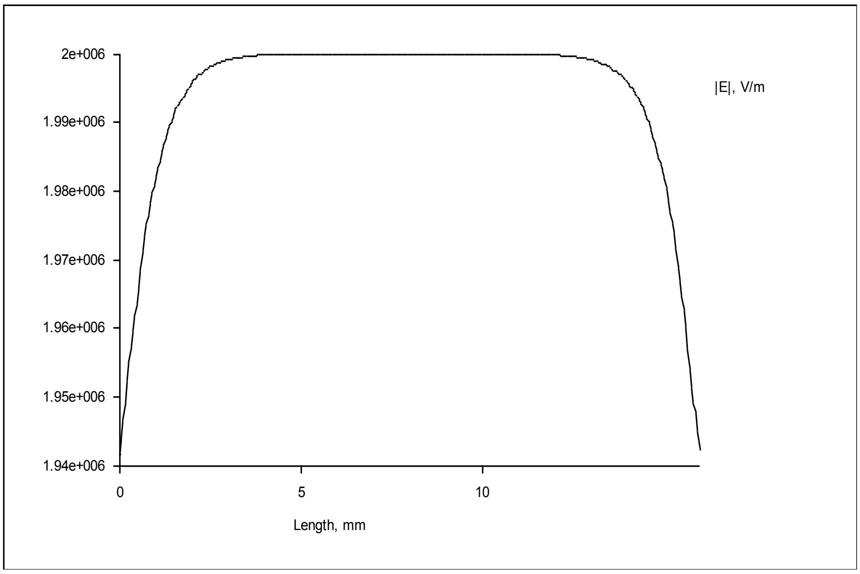

Figure 7 The distribution of the electrical intensity within a central section between the armatures, which is parallel to these

It is to be noticed that the values of the electric field intensity between the armatures, in their central area, where the uniform field appreciation is real, are of *20 KV/cm*, the same as they are when using the analytical formula.

The problem with the difference between the analytical solution and the numerical one becomes more obvious when evaluating the electrical charge.

The marking of the integration outline , in the FEM post processing page, is to be seen in *fig. 8,* whereas the results to the electrical charge calculations, made both ways, are presented (including the error percentage between the two) in *table 1*.

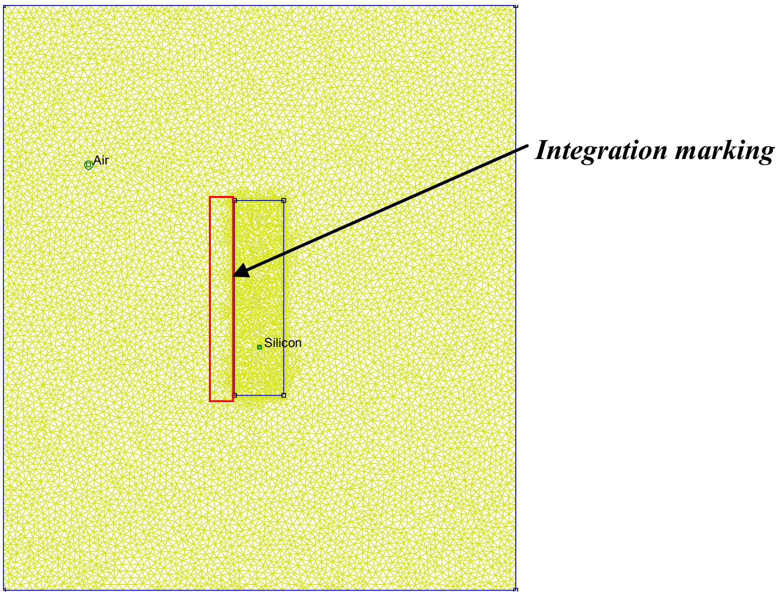

Figure 8. The marking of the integration outlinefor calculating the electrical charge

The FEMM 4.2 software, though two-dimensional, makes the transposition of line or surface integrals, into surface or volume integrals by setting a field at the same time with defining the problem referring to the depth of the plane parallel model, according to the *oz* axis.

Table 1. The values of the electrical charge, through FEM and analytical calculations

Relative permittivity	Q calculated through FEM	Q calculated analytically	Error percentage
-	[C]	[C]	[%]
1	6.06074E-09	4.52707E-09	25.30
3	1.51567E-08	1.35812E-08	10.39
6	2.87685E-08	2.71624E-08	5.58
12	5.59755E-08	5.43249E-08	2.95

The evolution of the error percentage from 25% to 3%, as the electric permittivity increases is normal, it is generated by the accentuated presence of the edge effect, if the dielectric and the environment are comparable.

The FEM analyses of the plane capacitors with liniar, isotropic and homogenous dielectric have been required, firstly, by the necessity to establish optimal values for the quantities influencing the FEM analysis (number and density of the elements on certain subfields, materials setting, bordering conditions, etc) and, secondly, by the necessity to offer value to some quantities which should allow their report in the studies to be made on non-homogenous dielectrics.

1.6. The study, through FEM, of the plane capacitor with liniar, isotropic and non-homogenous dielectric, in layers

The purpose of studying the plane capacitor, through FEM, presented in this paper,is to establish the stress to which the dielectrics may be subject to, in daily practice, and the influence that their superposition in an electric field has, on each of them.

As it is already known, the dielectrics used in daily practice are not ideal ones.They have a certain electrical conductivity, due mainly to their own ions or to the impurities they may contain. If the applied or the intensity of the electric field exceed certain values, it may appear in the dielectric a disruptive electrical discharge called breakdown. The maximal value of the intensity of the electric field which may be found inside a dielectric before its breakdown is called dielectrical rigidity (E_{str}). This item, specific to every dielectric, is determined experimentally, within the specified conditions that make it valid. The dielectrical rigidity relies on a series of factors , such as pressure, form and distance between the electrodes producing the breakdown (for the gasous ones), impurities, etc.

In *table 2.* , we are given the values of the dielectrical rigidity for some materials (Mocanu, 1981):

Table 2. The values of the dielectrical rigidity for some materials:

Dielectric	*Dielectrical rigidity [KV/cm]*	*Dielectric*	*Dielectrical rigidity [KV/cm]*
Air	*32*	*Rubber*	*400*
Mineral oil	*120 – 150*	*Cellulose*	*300 – 400*
Paraffin	*200 – 300*	*Mica*	*850 – 1200*
Polyethylene	*400*	*Porcelain*	*300 – 350*
Polystyrene	*200 - 300*	*Bakelite*	*300 -400*

The exposure of some dielectrics to certain amounts of stress may be done only after a careful study, which today is made mainly by numerical methods, the most commonly used being *The Finite Element Method*.

A research will be conducted, to establish the influence of introducing, between the armatures of a plane capacitor in air of a dielectric having the electrical permittivity $\varepsilon_r>1$, being parallel to the armatures and glued to one of them, leaving, however, some empty space between the armatures . The geometry of the capacitor is the one stated in the previous paragraph, the extra notes being : *1* – the air dielectric and *2*- a different dielectric, *fig. 9.*

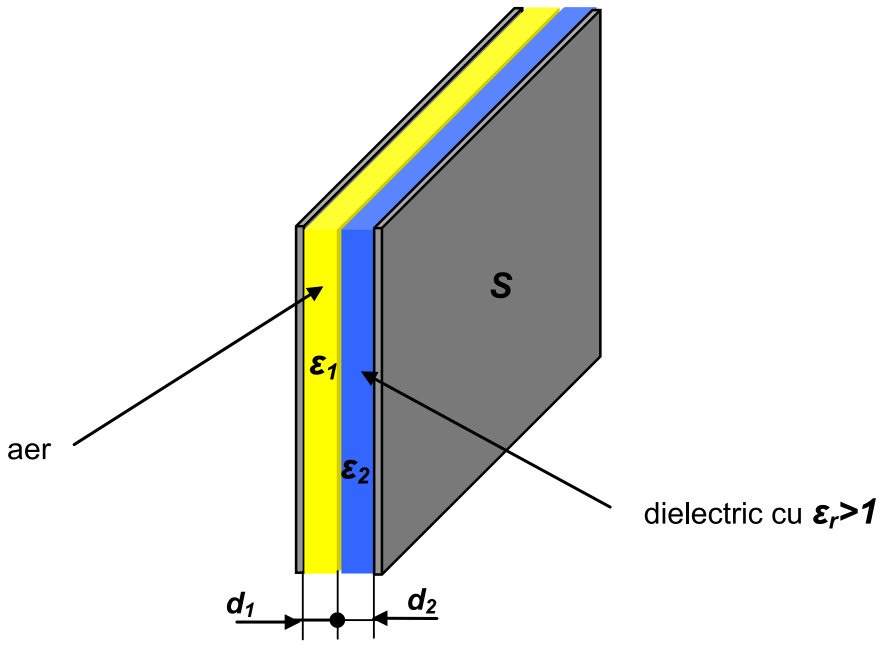

Figure 9. The plane capacitor with two parallel dielectrical layers

The study is based on the results found after FEM post processing of the configurations resulted from the following combinations:

1. air and rubber,
2. air and mica,
3. air and silicone.

For each of the three dielectric distributions , we will analyse the models to which the thickness of the air between the left armature and the dielectric, d_1, varies between half the distance between the armatures, that is *2mm* and *0,5mm* , with a *0,5mm* pace.

In order to avoid the abundance of data and figures, it will only be recorded the map of the equipotential lines and the distribution of values for the electric field intensity on the symmetry axis of the capacitor, data which are necessary for the quantitative and qualitative illustration of the reciprocal influence that the dielectrics have, when introduced in the electrical field.

The principles of the initial meshing network refinement, offered by the device, are identical with those mentioned in the previous paragraph, the settings of the air-dielectric separation surface, parallel with the armatures, being also done for very small element dimensions, as shown in *fig. 10,* in the case of of the air-rubber dielectric, with $d_1 = 1mm$.

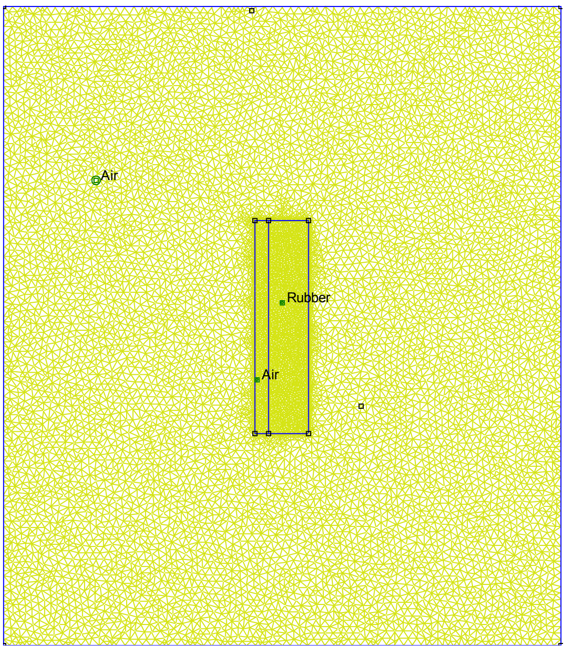

Figure 10. Refined meshing for the capacitor with air-rubber dielectric and thickness of the air layer of 1mm.

For this same model, the mapping of the equipotential lines reveals a concentration of the electric field in the air dielectric area, to the disadvantage of the rubber dielectric, *figure 11*. Obviously, this phenomenon comes with an increase of the electrical sollicitation on the air layer.

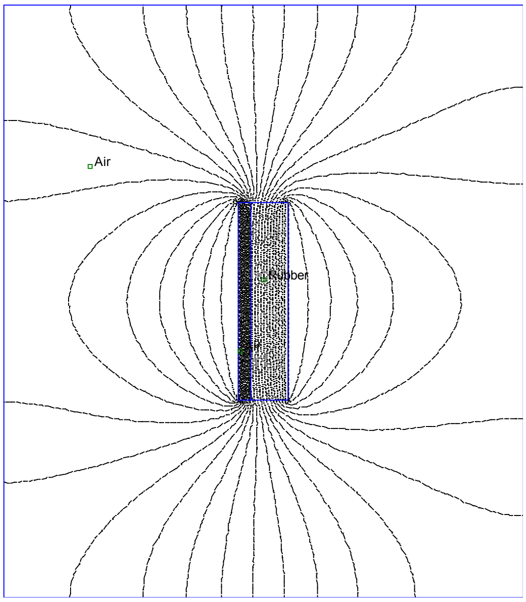

Figure 11. The equipotential lines for the capacitor with air-rubber dielectric and thickness of the air layer of 1mm.

By showing the distribution of the values attributed to the intensity of the electric field on the symmetry axis of the capacitor, *figure III.32*, one may easily notice the spectacular leap made by the intensity of the field when passing from one dielectric to the other.Thus, the values we refer to are *40 KV/cm* in air and *13,35 KV/cm*, in rubber. The constant aspect on the two levels is obviously justified by the position of the line on which the distribution was shown , that is an area with practically uniform electric field. Except for some corner areas, these values are the maximum values of the electric field intensity and they represent the basis of the dielectric sollicitation appreciation.

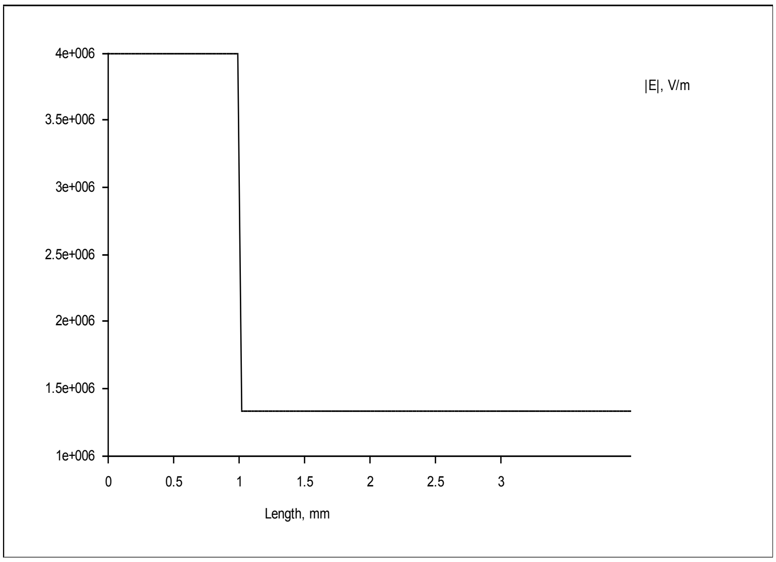

Figure 12. The distribution of the electric field intensity valueson the symmetry axis of the capacitor with air-rubber dielectric and the thickness of the air layer of 1mm.

The same figures are presented in Annex 3 for all the analysed configurations, but, in order to conclude the research in the present paper, we will put in a table only the values of the electric field intensity to be found in the air and in the dielectric, for all the combinations and all sizes of the air layer and type of dielectric analysed, *table 3*.

In all the possible combination of a dielectric with an air layer, we may notice the substantial modification of the electric field from the capacitor –meaning a raise of the stress level on the one with lower electrical permittivity. Taking into account the initial aspect of the field, before introducing the dielectric(see the previous paragraph), one may notice , in all the cases, an increase of the electrical field intensity in the air and a decrease in the dielectric we have introduced.

Table 3. The intensity of the electric field for the analysed configurations

d_1 [mm]	E_1 [KV/cm]			E_2 [KV/cm]		
	$\varepsilon_r = 3$	$\varepsilon_r = 6$	$\varepsilon_r = 12$	$\varepsilon_r = 3$	$\varepsilon_r = 6$	$\varepsilon_r = 12$
4	20	20	20	-	-	-
2	30	34.29	36.92	10	5.72	3.08
1.5	34.27	41.81	46.68	11.44	6.97	3.92
1	40	53.32	63.94	13.33	8.91	5.35
0.5	47.92	73.87	100.1	16.01	12.35	8.44

The lowest dielectrical rigidity may be found in the air, of all the dielectric layers that exist between the armatures of the analysed plane capacitors (*table 3),* therefore none of the non-air dielectrics is going to stand solicitations which are close to this value, especially since the values of the electrical intensity lowers in these dielectrics compared to the capacitor that has an air layer between the armatures, that is compared to the value of *20 KV/cm, figure 13*.

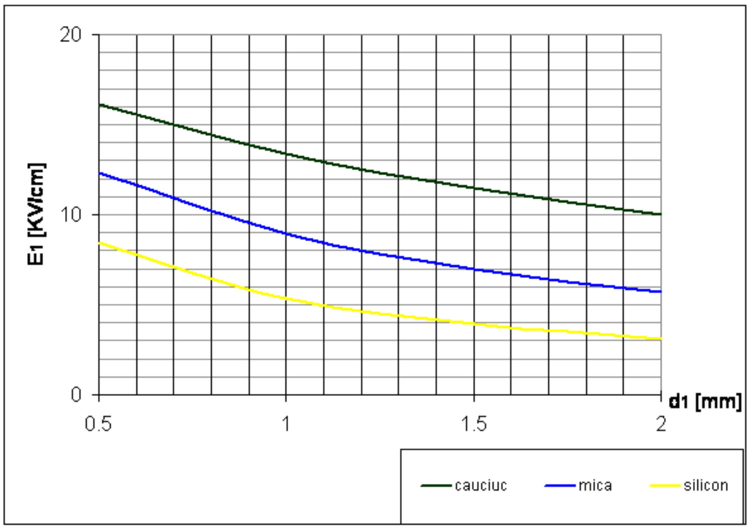

Figure 13. The dependence of the electric field intensityin the dielectric in relation with the size of the air layer, having as parameter the type of dielectric material introduced between the armatures

We may notice, however, the higher values of the electric field intensity in the dielectrics with lower permittivity, such as rubber and mica, opposed to the silicone.

By interpreting the data resulted from the FEM analyses, it has been noticed the strong solicitation to which is subdued an air layer, if we introduce between the armatures of a capacitor a dielectric having $\varepsilon_r > 1$, so that it does not completely fill the space between the armatures. The graphic representation of the data in the *table 3* ,referring to the air area on which we superpose the value of of the dielectrical rigidity of the air, under atmospheric pressure, offers a very clear figure of this problem, *figure 14*.

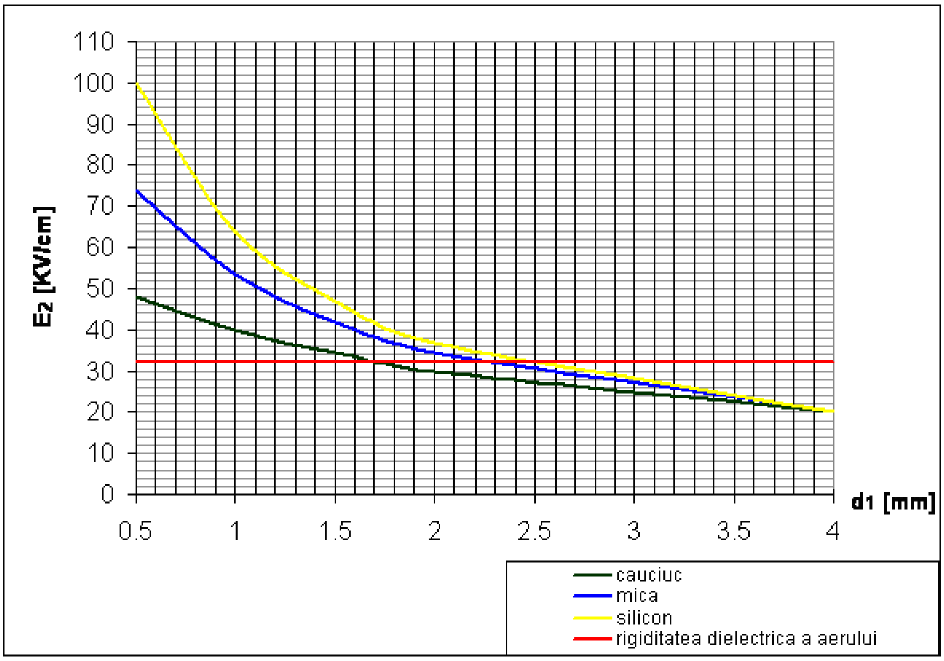

Figure 14. The dependence of the electric field intensity from the air to the size of the layer, having as parameter the type of dielectric material introduced between the armatures

Thus, by introducing a dielectric material, rubber, between the armatures of the plane capacitor, the breakdown of the air interstice between the left armature and the rubber will occur if the interstice size drops is under *1,7mm*. The value reached by the electric field intensity in an air layer of *0,5mm* is *47,92 KV/cm*, much higher than the breakdown value.

The situation gets worse if the dielectric materials used are mica and the silicone. The minimum layer of air that does not breakdown is *2,25mm*, respectively *2,5mm*, and the values reached by the electric field intensity inside the air layer of *0,5mm* are *73,87 KV/cm,* respectively *100,1 KV/cm.*

The study of the plane capacitor , with liniar, istrope and homogenous/non homogenous dielectric ,finalised with the raise of the dependence of the electric field intensity in air on the size of the air layer and having as parameter the type of dielectric material introduced between the armatures, is an example of confirmation or invalidation of the possibility and utility of using layers of dielectrics between the armatures of the capacitors.

By making a report of all the values of the elements inherent to the capacitor with a homogenous dielectric, having an electrical permittivity ε_2 and defining the equationt k:

$$k = \frac{\varepsilon_2}{\varepsilon_1} \tag{III.20}$$

the results may be extended for any dielectric material combinations, *figure 15.*

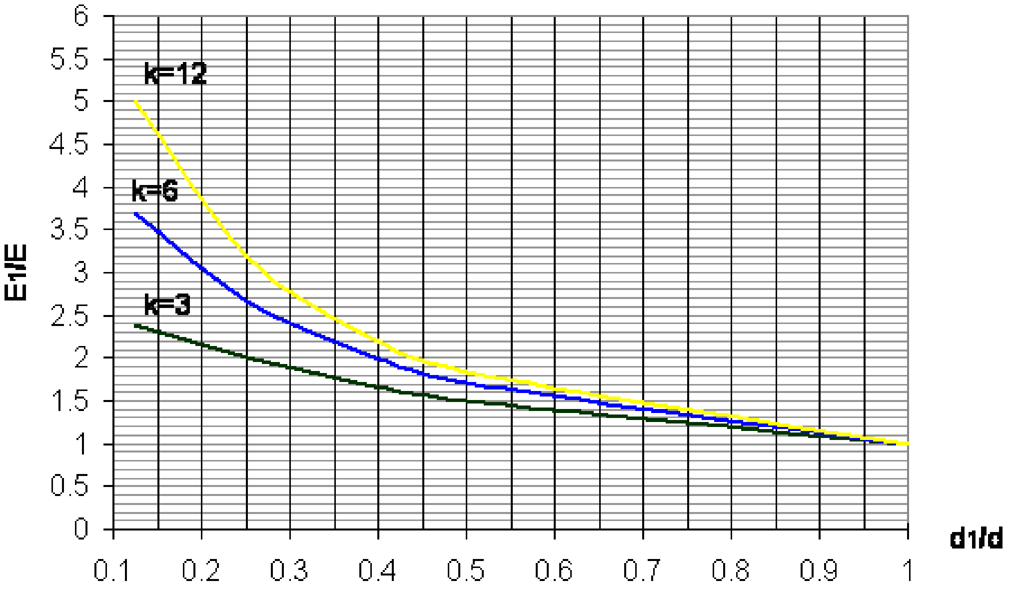

Figure 15. The dependence of the relative electric field intensity in the dielectric layer on the lowest permittivity, in relation with the size of the layer and having as parameter the K equation

2. CONCLUSIONS

It was illustrated the necessarily steps in Finite Element Method analysis of an electrostatic problem. Setting the geometry, choosing the materials, the meshing refinement, proper choosing of boundary conditions are some of them.

Also it was outlined the Finite Element Method educational potential due to the illustrative results.

Finaly, the general form of the the dependence of the relative electric field intensity in the dielectric layer on the lowest permittivity, in relation with the size of the layer and having as parameter the K equation it was produced.

REFERENCES

1. Binns K. J, Lawrenson P. J, Trowbridge C. W. *The analytical numerical solution of electric and magnetic fields*, Oxford: Pergamon Press, 1963.
2. Chari M.V.K, Silvester P.P. *Finite elements in electrical and magnetic field problems*, London: Mc Graw-Hill, 1980.
3. Chen Q, Konrad A.. *A review of finite element open boundary techniques for static and quasistatic electromagnetic field problems*, IEEE Trans. on magnetics, vol. 33, nr.1, 663-676, 1997.
4. Freeman E, Lowther D. . *A novel mapping technique for open boundary finite element solutions to Poisson's equation*, IEEE Trans. on magnetics, vol. 24, nr.6, 2934-2936, 1998.
5. Jianming Jin. *The Finite Element Method in electromagnetics*, New York: John Wiley & Sons inc., 1993.
6. Silvester P.P, Ferrari R.L. *Finite elements for electrical engineers - Second edition*, Cambridge University Press, 1990
7. Simion E, Maghiar T. *Electrotehnică*, Bucureşti: Ed. Didactică şi Pedagogică, 1981.
8. Şora Ctin.. *Bazele electrotehnicii*, Bucureşti: Ed. Didactică şi Pedagogică, 1982.

STUDY OF A PHOTOVOLTAIC SYSTEM WITH MPPT USING MATLAB^{TM}

Dumitru **POP**, Radu **TÎRNOVAN**, Liviu **NEAMŢ**, Dorin **SABOU**
Technical University of Cluj Napoca
dan.pop@enm.utcluj.ro

Key words: photovoltaic system, solar irradiation, modeling, simulation
Abstract*: In this paper a photovoltaic (PV) system is analyzed using Matlab. First, a Matlab code is written in order to obtain the I-V and P-V curves at different values of solar irradiation and cell temperature. The results were compared with the experimental data of a commercial PV module, USP 150. Then, the code was implemented in Simulink and, along with a MPPT algorithm and a DC-DC converter, the whole system was simulated.*

1. INTRODUCTION

In the last years, the use of alternative energy sources in electricity supply systems has rapidly increased. The increasing interest for renewable energies is due to the increasing concerns about fossil fuel deficit, high oil prices, global warming, and damage to environment and ecosystem. Also, another advantage of renewable energies is that it is suitable for electrifying remote areas where the electric grid does not reach and it is also becoming an economically viable renewable power source for distributed generation.

Solar energy, wind energy, hydro-power, bio-gas energy etc. are the most popular renewable energy sources. Research and development in each of these areas is being carried out in all parts of the world, out of which the solar energy is one of the cleanest and the least expensive one. [1] Abundance and sustainability of solar radiant energy are important factors that characterize the energy through the PV (photovoltaic) effect among the renewable energy resources. Regardless of the intermittency of sunlight, solar energy is widely available and completely free of cost. Despite of the high initial cost and low efficiency, PV system has small operation and maintenance costs as it is a stationary source of energy fabricated from semiconductor material. [2] The output characteristics of PV module depends on the solar irradiation, the cell temperature and output voltage of PV module. Since the PV has a nonlinear current-voltage (I-V) characteristic, it is vital to model the PV unit for MPPT (maximum power point tracking) in PV-based power systems, [3].

2. PV MODEL DEVELOPMENT

A PV module consists of a number of solar cells connected in series and parallel to obtain the desired voltage and current output levels. Mostly commercial modules consist of 36 or 72 cells.

During darkness, the solar cell is not an active device and it works as a diode with a p-n junction. It produces neither a current nor a voltage. As sunlight strikes a solar cell, the incident energy is converted directly into electrical energy without any mechanical effort. Transmitted light is absorbed within the semiconductor, by using this light energy to excite free electrons from a low energy status to an unoccupied higher energy level. When a solar cell is illuminated, excess electron-hole pairs are generated throughout the material, hence the p-n junction is electrically shorted and current flows. [4]

The simplest equivalent circuit of a solar cell is a current source in parallel with a diode. (Fig. 1) The output of the current source is directly proportional to the light falling on the cell (photocurrent I_L).

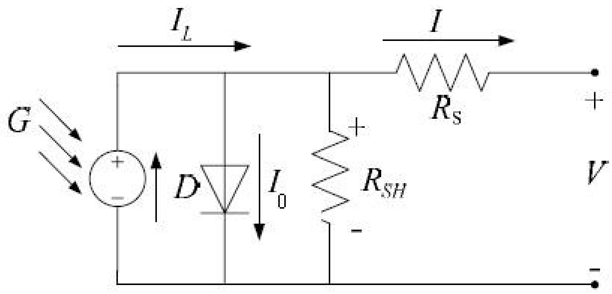

Fig. 1 – The equivalent circuit of a PV cell

The symbols in Fig. 1 are defined as follows: G – solar irradiation, I_L – photocurrent, D – diode, I_0 - the diode saturation current, R_{SH} – the shunt resistance, R_S - series resistance, I – the net current of the solar cell and V – the voltage of the solar cell.

Shunt resistance R_{SH} corresponds to the leakage current to the ground (is commonly neglected) and the series resistance R_S represents the internal losses due to the current flow. In an ideal cell, $R_{SH}=R_S=0$.

The net current of the cell is the difference of the photocurrent, I_L and the normal diode current I_0:

$$I = I_L - I_0(e^{\frac{q(V+IR_S)}{nkT}} - 1) \quad (1)$$

where:

- q = 1.6 X 10^{-19} [C] – the electron charge;
- k = 1.38 X 10^{-23} [J/K] – the Boltzmann's constant;
- T - the cell temperature [K];
- n – the diode quality factor.

The temperature dependence of the photocurrent I_L and the saturation current of the diode I_0 [5]:

$$I_L = I_L(T_1) + K_0(T - T_1) \quad (2)$$

$$I_L(T_1) = I_{SC}\left(T_{1,nom}\right)\frac{G}{G_{nom}} \quad (3)$$

$$K_0 = \frac{I_{SC}(T_2) - I_{SC}(T_1)}{T_2 - T_1} \quad (4)$$

$$I_0 = I_0(T_1) \times (\frac{T}{T_1})^{\frac{3}{n}} e^{\frac{qV_g(T_1)}{n\,k\,(\frac{1}{T} - \frac{1}{T_1})}} \quad (5)$$

$$I_0(T_1) = \frac{I_{SC}(T_1)}{(e^{\frac{q\,V_{oc}(T_1)}{n\,k\,T_1}} - 1)} \quad (6)$$

$$R_S = -\frac{dV}{dI_{Voc}} - \frac{1}{X_V} \quad (7)$$

$$X_V = I_o(T_1)\frac{q}{nkT_1}e^{\frac{qV_{oc}(T_1)}{nkT_1}} - \frac{1}{X_V} \quad (8)$$

$$V_{oc} = \frac{nkT}{q}\ln\left(\frac{I_L}{I_0}\right) = V_t \ln\left(\frac{I_L}{I_0}\right) \quad (9)$$

where

- I_{sc} – is the short circuit current [A];
- V_g is the band-gap energy of the semiconductor used in the cell [eV];
- V_{oc} - open circuit voltage [V].

3. SIMULATION AND RESULTS

In this paper a PV module fabricated by Udhaya Semiconductors Limited is analyzed. Table1 presents the specifications of the USP150 PV module standard test conditions (STC), which means an irradiation of 1000 W/m^2 with an AM1.5 spectrum at 25° C . The values were obtained from the manufacture's datasheet.

Table1. Parameters of the USP150 module

Maximum Power	*150 W*
Open Circuit Voltage (Voc)	*43 V*

Maximum power point voltage (Vmpp)	*33,5 V*
Short circuit current (Isc)	*4,9 A*
Maximum power point current (Impp)	*4,5 A*
No. of cells	*72*
Configuration	*24 V*
Maximum system voltage	*1000 V*
Type of Solar Cell	*mono-Si*

In order to analyze the solar cell behavior at different solar irradiation or temperature, a code was written in Matlab which use the solar script developed by González-Longatt in [5]. The screen shot of the code is presented in Fig. 2.

```
% Behavior at different solar irradiation or temperature of USP150 PV module
data = xlsread('USP150.xlsx', 'Data', 'A:B'); %Read curve's points from the Excel file
dataU = data(:,1);% Extract Voltage of the PV module
dataI = data(:,2);% Extract Current of the PV module
clear data

% Cell computation
dataUcelula=dataU/72;% Voltage of the solar cell
Va =dataUcelula';
Ia0=solar(Va,1,25); %Current of the solar cell

% Panel computations:
Ns = 72; % Number of cells serially connected in a panel [].
Va0 = 0:0.01:0.665; % Voltage vector of one cell [V]
Ia1 = solar(Va0,1,25); % Compute current from voltage vector [A]
Va1 = max(Ns*interp1(Ia1, Va0, 0:0.001:ceil(max(Ia1)*100)/100, 'linear', 'extrap'), 0);
Ia2 = solar(Va0,1,50);
Va2 = max(Ns*interp1(Ia2, Va0, 0:0.001:ceil(max(Ia2)*100)/100, 'linear', 'extrap'), 0);
Ia3 = solar(Va0,0.8,25);
Va3 = max(Ns*interp1(Ia3, Va0, 0:0.001:ceil(max(Ia3)*100)/100, 'linear', 'extrap'), 0);
Ia4 = solar(Va0,0.5,25);
Va4 = max(Ns*interp1(Ia4, Va0, 0:0.001:ceil(max(Ia4)*100)/100, 'linear', 'extrap'), 0);
Ia5 = solar(Va0,0.2,25);
Va5 = max(Ns*interp1(Ia5, Va0, 0:0.001:ceil(max(Ia5)*100)/100, 'linear', 'extrap'), 0);
RelativeError=abs((dataI-Ia0')./dataI);
```

Fig. 2 – The code written in Matlab in order to analyze the behavior of PV module

Below are presented the results of the Matlab code: Fig 3 presents the I-V curve of solar cell at STC and at different values of the temperature, Fig. 4 presents the P-V curve at different irradiation values and temperatures, Fig. 5 presents the I-V curve of the PV module at different values of temperature and solar irradiation and Fig. 6 presents the relative error between the I-V curve provided by the manufacturer and the I-V curve obtain with the Matlab code.

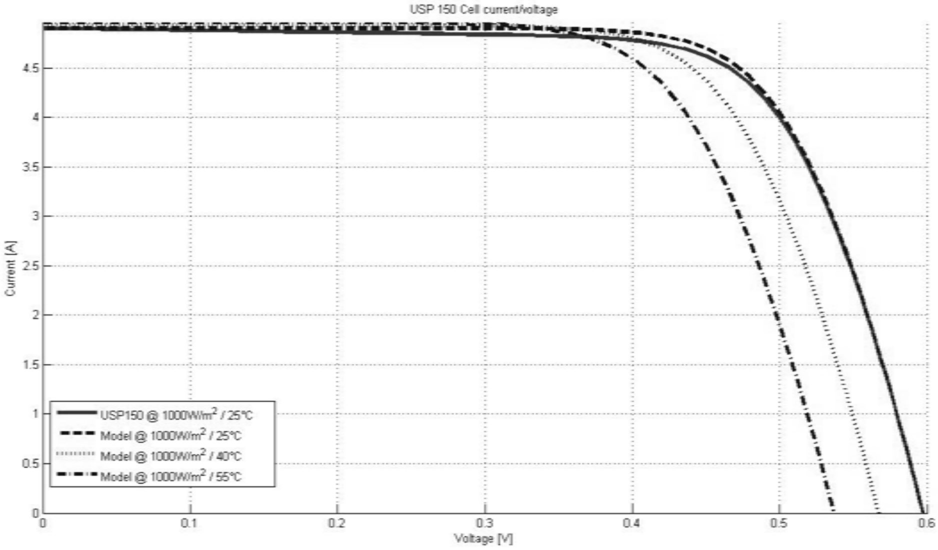

Fig. 3 – The I-V curve of the solar cell obtained with the Matlab code

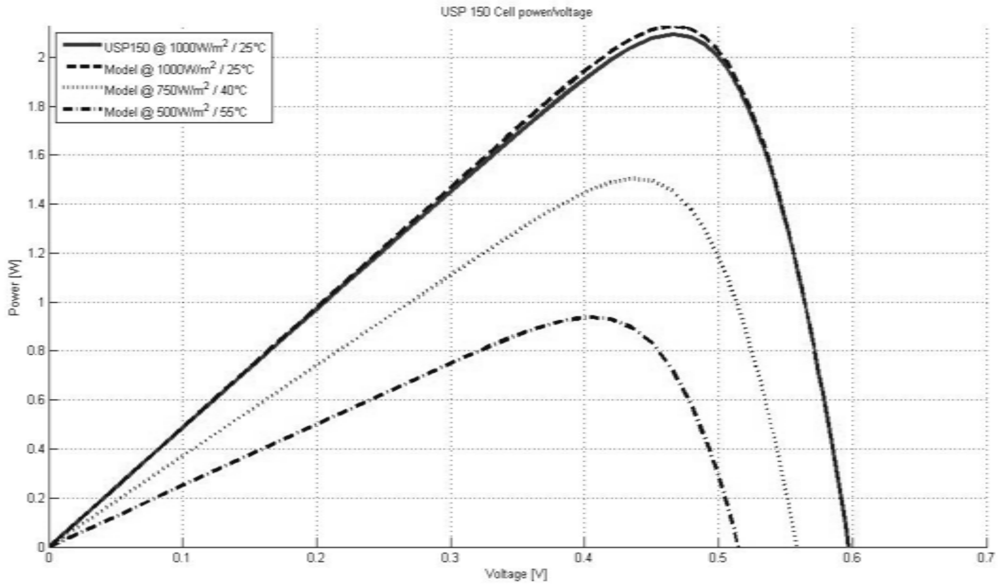

Fig. 4 – The P-V curve of the solar cell obtained with the Matlab code

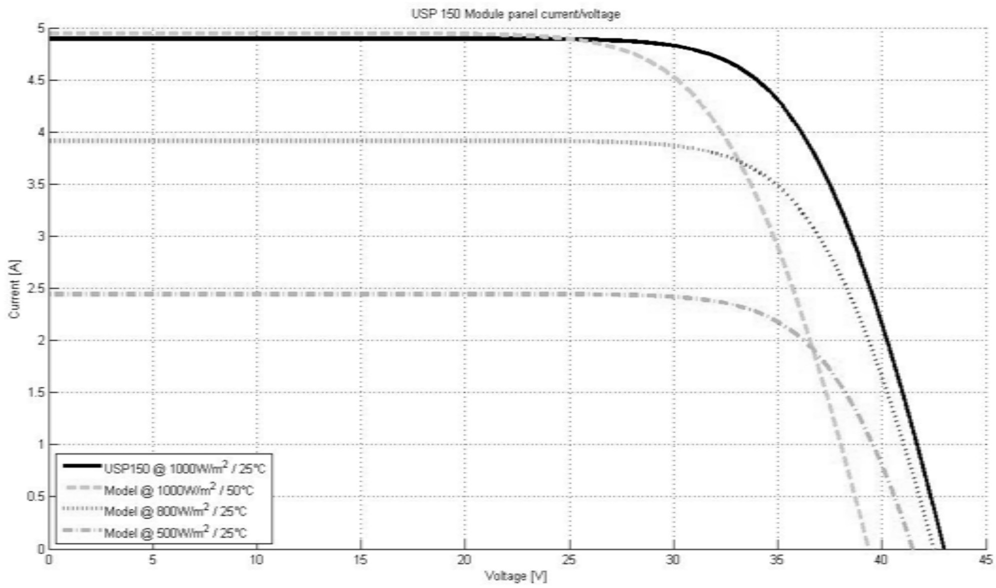

Fig. 5 – The I-V curve of the PV module obtained with the Matlab code

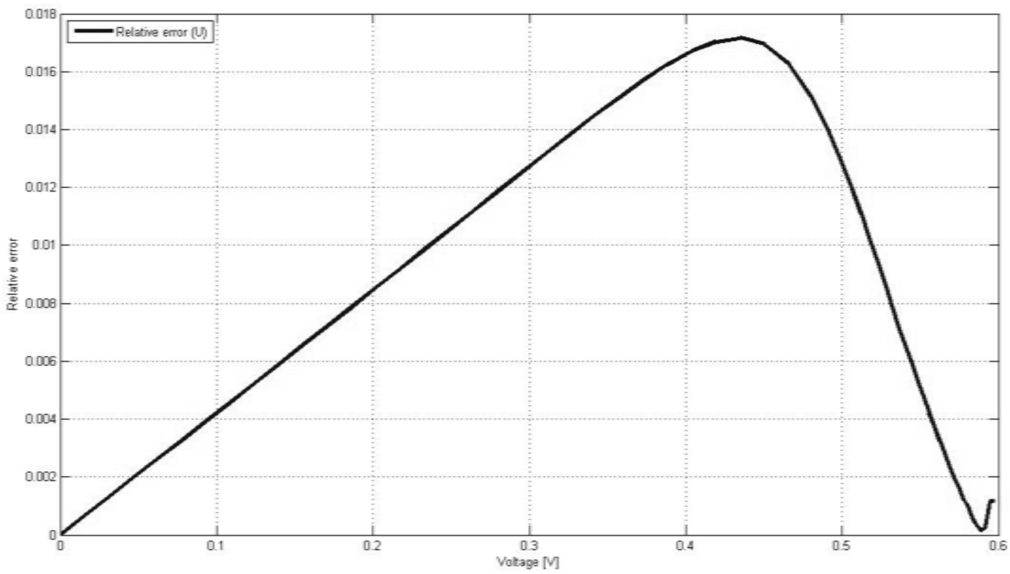

Fig. 6 – The relative error between the real and obtained I-V curve

With the variation of irradiation and temperature, the power output of PV module varies continuously. The maximum power point tracking (MPPT) algorithm is used for extracting the maximum power from the solar PV module and transferring that power to the load. By changing the duty cycle of the PWM control signal, the load impedance as seen by the source varies and matches the point of the peak power of the source so as to transfer the maximum power. The perturbation and observation (P&O) method has been widely used because of its simple feedback structure and fewer measured parameters. The peak power tracker operates by periodically incrementing or decrementing the solar array voltage. If a given perturbation leads to an increase (decrease) in array power, the subsequent perturbation is made in the same (opposite) direction. In this manner, the peak power tracker continuously hunts or seeks the peak power conditions. [6] The flow chart of the P&O algorithm is shown in Fig. 7

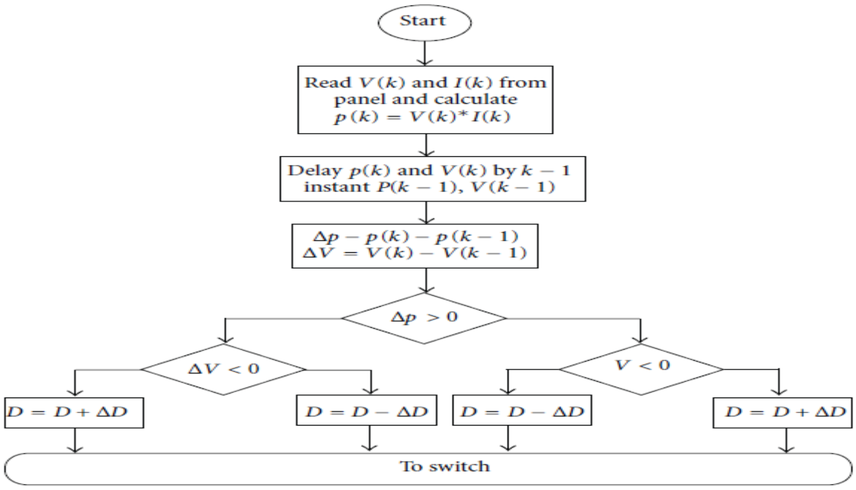

Fig. 7 – The flow chart of the P&O algorithm

In Fig. 8 is presented the PV system created in Matlab – Simulink.

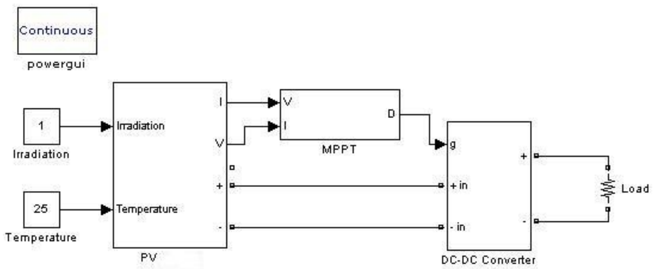

a) The PV system created in Simulink

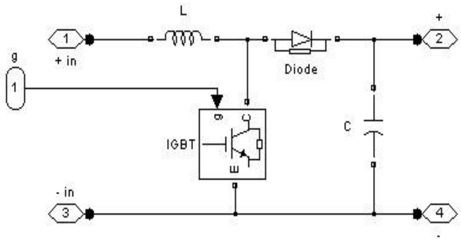

b) The DC-DC converter subsystem

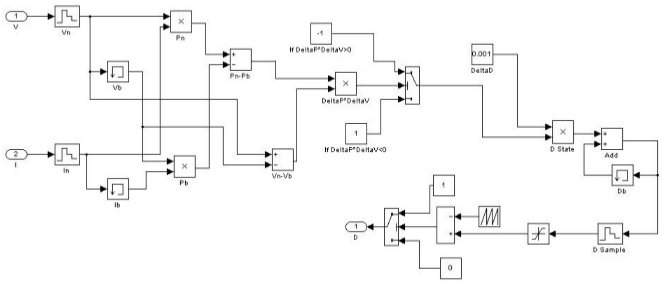

b) The MPPT subsystem

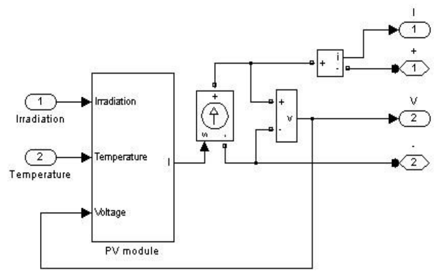

d) The PV subsystem

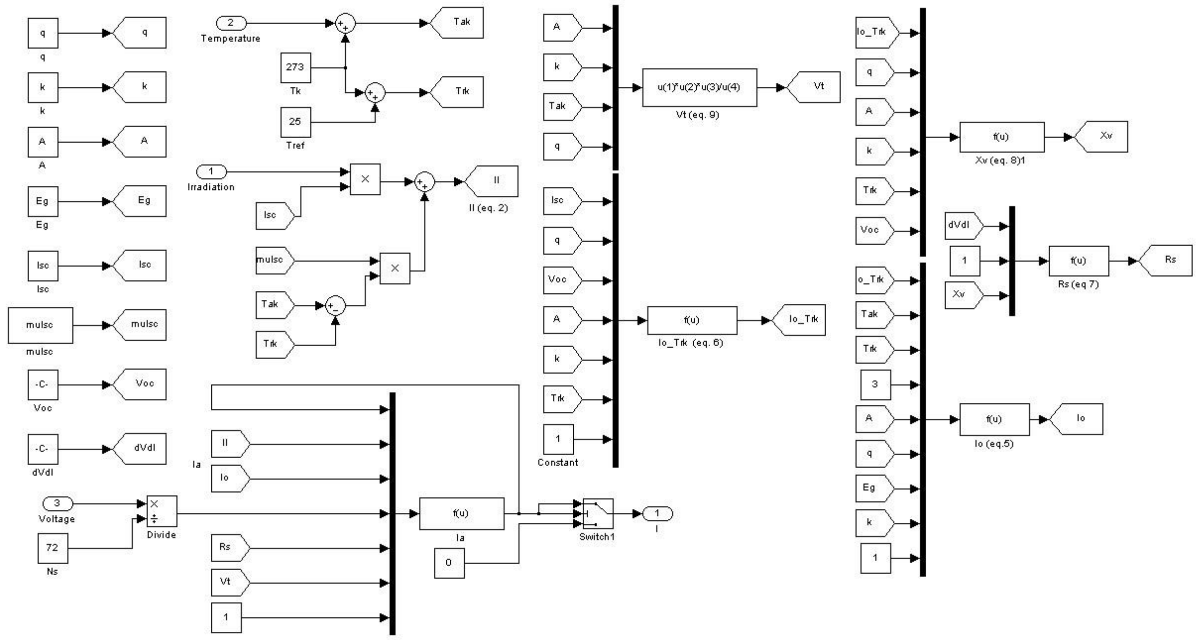

e) The PV module subsystem

Fig. 8 –The PV system created in Matlab - Simulink

Fig. 9 presents the voltage at the input and output of the DC-DC converter obtained after the simulation.

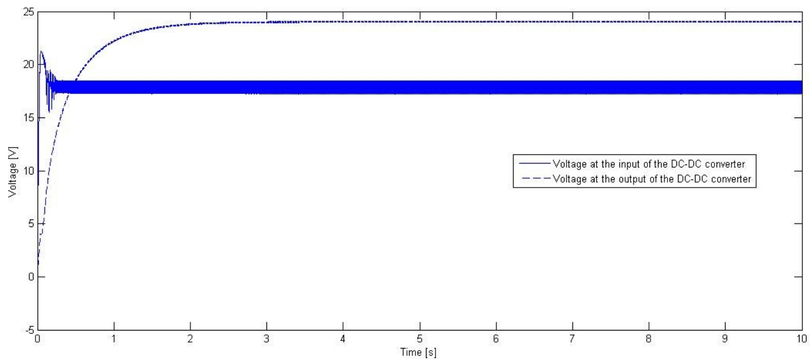

Fig. 9 –The voltage at the input and output of the DC-DC converter

3. CONCLUSIONS

In this paper, a Matlab code was written in order to analyze the behavior of a commercial PV module and the results were compared with the data from manufacture's datasheet. Then, it was implemented in Matlab-Simulink, along with a MPPT algorithm and a DC-DC converter. The inputs of the developed model using SimPowerSystems toolbox are solar irradiation and PV array operating temperature. The purpose of the MPPT is to adjust the solar operating voltage close to the MPP under changing atmospheric conditions. The DC-DC converter provides a constant voltage output.

ACKNOWLEDGMENT: This paper was supported by the project "Improvement of the doctoral studies quality in engineering science for development of the knowledge based society-QDOC" contract no. POSDRU/107/1.5/S/78534, project co-funded by the European Social Fund through the Sectorial Operational Program Human Resources 2007-2013.

REFERENCES

1. D. Jose*, Comparison of a Three Phase Single Stage PV System in PSCAD and PowerFactory, Degree* project, School of Elect. Eng., KTH Royal Institute of Technology, Stockholm, Sweden, 2012.
2. S. Samer, M. Ahmed, et. al., *A Matlab/Simulink-Based Photovoltaic Array Model Employing SimPowerSystems Toolbox*, Journal of Energy & Power Engineering, Vol. 6 Issue 12, p1965, 2012.
3. H. Tsai, C. Tu, Y. Su, *Development of Generalized Photovoltaic Model Using Matlab/Simulink*, Proceedings of the World Congress on Engineering and Computer Science, pp 846– 851, San Francisco, USA, 2008.
4. N. Pandiarajan, R. Ramaprabha, R. Muthu, *Application of Circuit Model for Photovoltaic Energy Conversion System*, International Journal of Photoenergy, 2012
5. F. González-Longatt, *Model of Photovoltaic Module in Matlab^{TM}*", 2DO Congreso Iberoamericano De Estuiantes De Ingenieria A Electrica, Electronica Y Computacion, pp. 1-5, 2005
6. C. Hua, C. Shen, *Study of maximum power tracking techniques and control of DC/DC converters for photovoltaic power system*, Power Electronics Specialists Conference, pp. 86 - 93, Fukuoka, 1998

OVERVOLTAGE SUPPRESSION IN INVERTER DRIVEN INDUCTION MOTORS

Ioan **ȚILEA**, Călin **MUNTEANU**
Technical University of Cluj-Napoca,
Ioan.Tilea@ethm.utcluj.ro

Key words: ***electromagnetic interference, inverter, induction motor, overvoltage suppression***
Abstract*:* *The motor overvoltage in inverter driven induction motors is one of the most difficult current technical problem in variable speed system. The conducted electromagnetic interference (EMI) in inverter driven motor system is essentially related to the electric behavior of the frequency converter`s load which is the induction motor and motor cable. Obtained results illustrate that the overvoltage problem in variable speed system with high power motors and long cables can be suppressed using the method presented in this paper that consists of a filter which bypasses the motor overvoltage to the ground.*

1. INTRODUCTION

The increase in the carrier frequency of pulse width modulation and fast switching rates of the power electronics can induce serious problems in inverter fed induction motor drive system. Many small capacitive couplings exist in the motor drive systems which may be neglected by the low frequency analysis but the conditions are completely different at high frequencies were the influence of the parasitic capacitance is noticeably higher. When the inverter is connected to the motor through a long cable because of the cable inductance, the stray capacitance distributed between the cable wires and the high rise times of the pulse width modulation (PWM) voltage from the inverter, overvoltages appear at the motor terminals, as presented in Figure 1, [1]-[4].

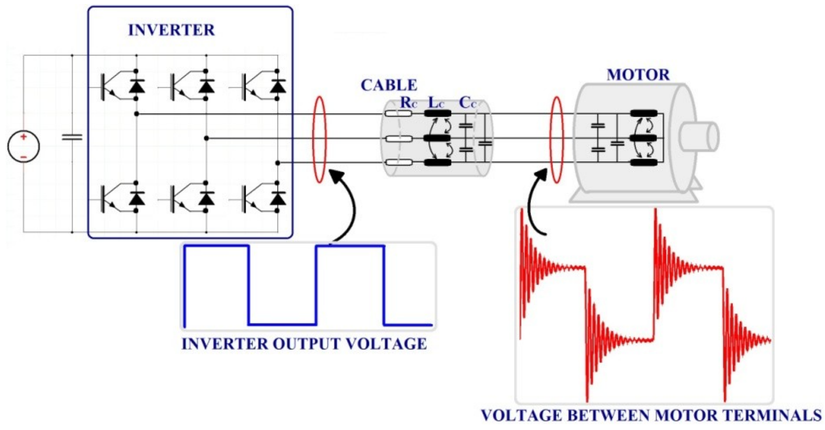

Fig. 1 – Motor terminal overvoltage

The cable and motor can be considered a resonant circuit, which is excited by the rectangular pulses of the inverter. The overvoltages at the motor terminals stress the motor winding insulation reducing its life, causing partial discharges that damage the insulation of the motor. This paper analyzes a new method for suppressing the overvoltage phenomenon in inverter driven induction motor system.

2. METHOD USED

For analyzing the motor terminal overvoltage propagation in inverter driven induction motors a field-circuit coupled method is used, first carrying out a finite element analyses of the investigated induction motor with a 3D software for the extraction of the motor high frequency equivalent circuit, using a 2D software for extracting the high frequency equivalent circuit of the cable and a circuit analysis for the inverter fed induction motor drive system.

Using the 3D software a finite element analysis of the induction motor is carried out to obtain the inductances and the capacitances of the induction motor necessary for the motor high frequency equivalent circuit, first performing a magnetic regime simulation for obtaining the inductance matrix and an electrostatic simulation for the capacitance matrix.

The induction motor inductances and capacitances obtained from the software's Matrix solution are exported in a circuit simulator, composing the high frequency equivalent circuit of the induction motor used for the inverter fed induction motor drive system to analyze the overvoltage phenomenon accruing at the motor terminals.

2. 1. Induction motor and cable model

At low frequencies, the equivalent circuit of the electric motor consists of inductances and resistances without considering the motor capacitances. At high frequencies, the electric motor can be modeled as distributed capacitors, inductors and resistors. The stray capacitance of electric motors is very important in predicting EMI problems, asynchronous motor winding physical construction is very complicated and detailed determination of its capacitance is difficult [5]-[8].

For an accurate determination of the induction motor capacitance and inductance a 3D model of the motor must be analyzed for the reason that it incorporates the end winding of the induction motor. The investigated motor is a three phase induction motor with a single layer winding and an output power of 0.3 kW, a rated voltage of 400 V and a speed of 1360 rpm. The numerical 3D model and a 2D section of the induction motor simulated is presented in Figure 2.

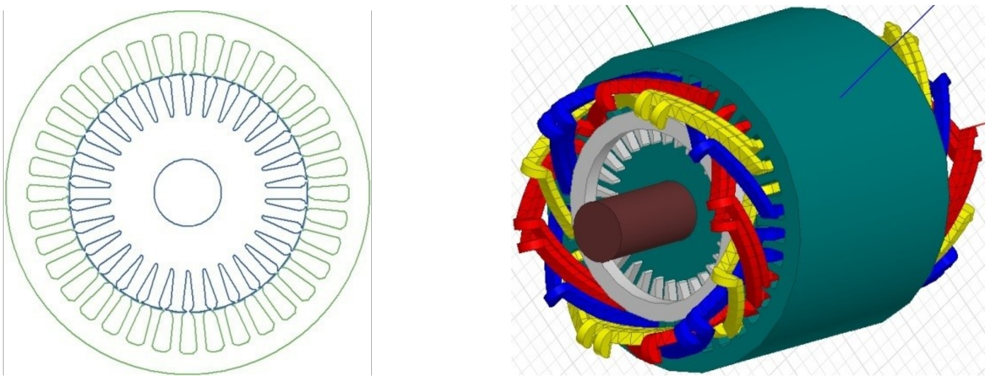

a) b)

Fig. 2 – Numerical model of the induction motor: a) 2D section, b) 3D model

The high frequency model of the motor cable is obtained by extracting the inductances and capacitance of the cable using a 2D software. Because the power cable that connects the motor to the inverter has a very simple physical construction a 2D model of the motor cable is use, the results from the magnetostatic simulation (Fig.3.a) and electrostatic simulation (Fig.3.b) are presented in Figure 3.

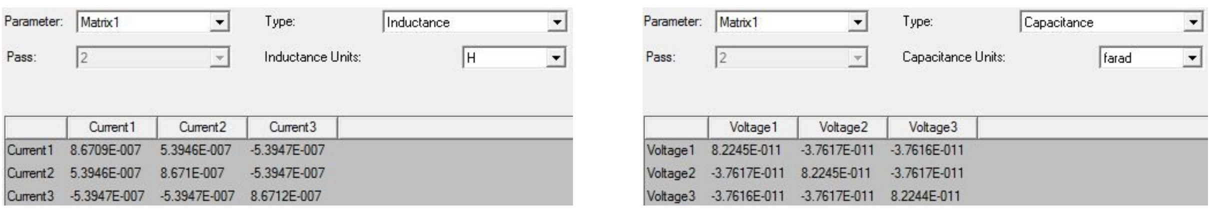

Parameter: Matrix1 Type: Inductance
Pass: 2 Inductance Units: H

	Current1	Current2	Current3
Current1	8.6709E-007	5.3946E-007	-5.3947E-007
Current2	5.3946E-007	8.671E-007	-5.3947E-007
Current3	-5.3947E-007	-5.3947E-007	8.6712E-007

Parameter: Matrix1 Type: Capacitance
Pass: 2 Capacitance Units: farad

	Voltage1	Voltage2	Voltage3
Voltage1	8.2245E-011	-3.7617E-011	-3.7616E-011
Voltage2	-3.7617E-011	8.2245E-011	-3.7617E-011
Voltage3	-3.7616E-011	-3.7617E-011	8.2244E-011

a) b)

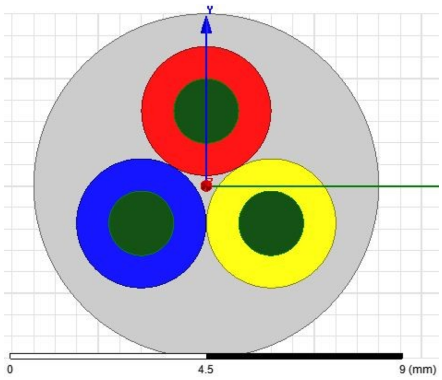

c)

Fig. 3 – Results of the motor cable simulations: a) Inductance Matrix; b) Capacitance Matrix; c) 2D model of the investigated motor cable

2.2. Overvoltage analysis and suppression in inverter driven induction motors

To analyze the overvoltages at the motor terminals when the motor is connected to a PWM inverter the simulation model presented in Figure 4, is used. The model consists of an inverter, the equivalent high frequency model of the cable composed of the inductances matrix and capacitances matrix imported from the 2D simulation and the induction motor capacitances matrix and inductances matrix imported from the 3D simulation which will compose the high frequency model of the induction motor.

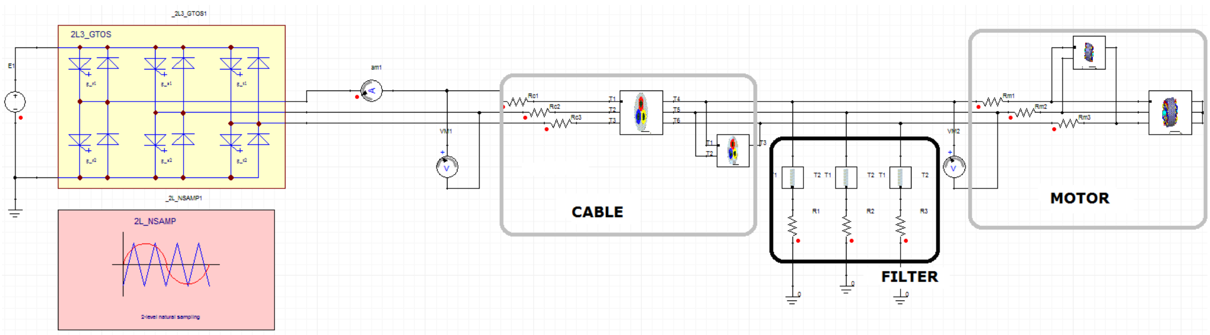

Fig. 4 – Inverter fed induction motor simulated model

The method for suppressing the overvoltage at the motor terminal consists of a filter that bypasses the motor overvoltage to the ground; the inverter-filter-motor layout is presented in Figure 4. The filter consists of a capacitor and a resistance, the values of the capacitor and resistor must be chosen in such a way that the series resonance of the motor and cable would be cancel so the cable and motor resonance phenomenon must be taken into account when choosing the values for the filter components.

3. RESULTS

In Figure 5 the motor terminal voltage, Fourier analysis of the voltage and a Bode plot of the motor current are presented, the overvoltage at the motor terminal is clearly visible with a peak amplitude of 1000 V, were the inverter output voltage presents no voltage spikes. The inverter output voltage has an amplitude of 500 V and a fundamental frequency of 50 Hz with a carrier frequency of 20 kHz and the induction motor is connected to the inverter through a 35 m cable. The induction motor behavior in high frequency is that of an LC parallel circuit having a parallel resonance at a frequency of 3.5 kHz, when the electrical parameters of the motor cable are taken into account besides a parallel resonance it can be observed that there are two series resonances at 300 kHz and at 700 kHz, the first series resonance (300 kHz) appear only if the motor cable model incorporates the cable mutual inductances. The series resonance of the motor and cable is very important in predicting serious overvoltage problems in inverter driven asynchronous motors, and it is the key reason for the appearance of motor overvoltage, as seen in Fig. 5 the frequency of the overvoltage at the motor terminal is 700 kHz the same as the second series resonance of the motor and cable, the resonance is due to the cable induction and motor winding capacitance.

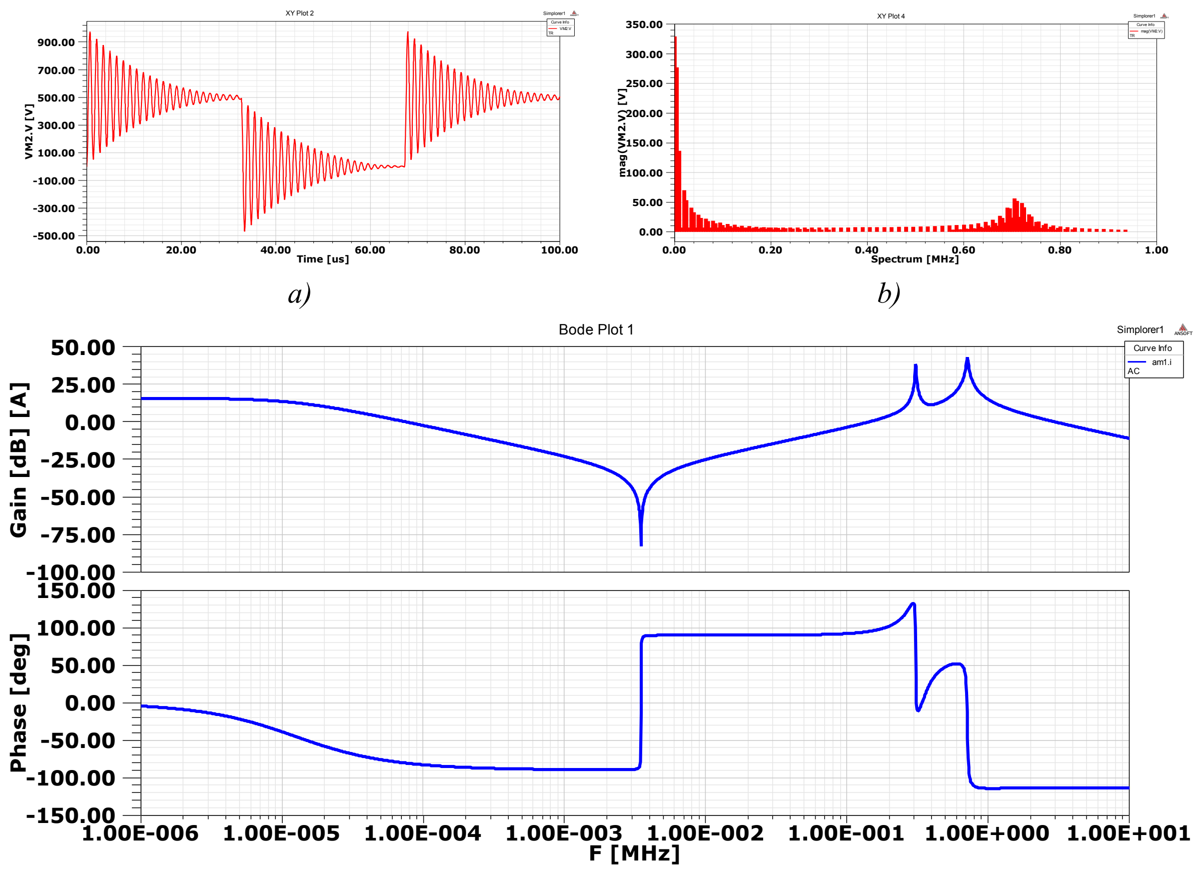

a) *b)*

c)

Fig. 5 – Results from the simulation without using the filter: a) Motor terminal voltage, b) Fourier analysis of the motor terminal voltage, c) Bode plot of the motor and cable.

In Figure 6 the motor terminal voltage, Fourier analysis of the voltage and a Bode plot of the motor current are presented when using the filter, the overvoltage suppression effect of the filter is clearly visible the maximum amplitude of the voltage at the motor terminal is reduce by 100 V and the number of the overvoltage oscillations are drastically reduce.

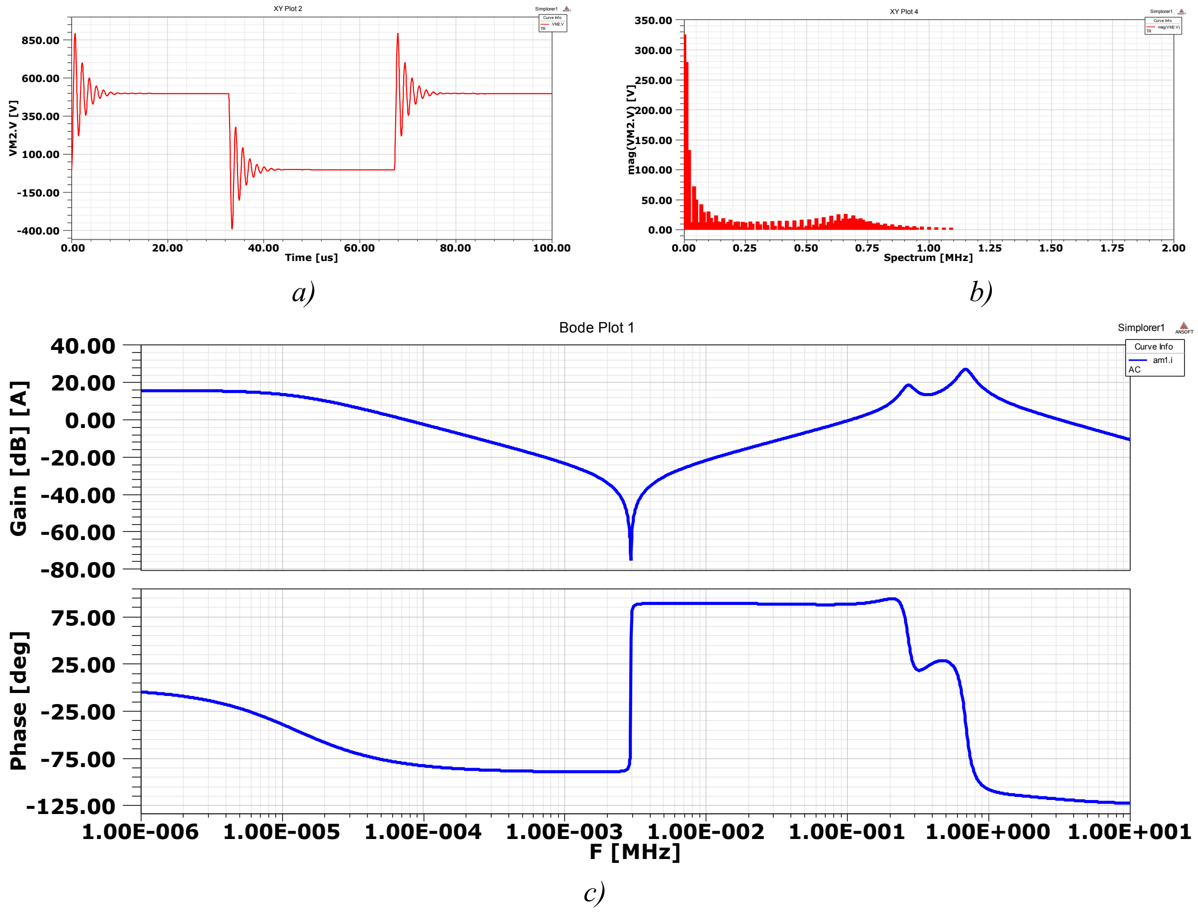

Fig. 6 – Results from the simulation using the filter: a) Motor terminal voltage, b) Fourier analysis of the motor terminal voltage, c) Bode plot of the motor and cable.

4. CONCLUSION

The characteristic frequency range where the overvoltage problems appear can be relatively easily determined based on the motor and cable resonant frequency. The series resonant frequency of the motor and cable is very important for the reason that the voltage spikes at the motor terminal have the same frequency. Determining the resonant frequency of the motor and cable is very helpful in predicting serious EMI problems in inverter driven motor system. Overvoltages in inverter fed induction motor system, with long motor cable can be predicted using the field-circuit coupled method presented in this paper.

At high switching frequencies the inverter power losses dramatically decreases so there is an interest in making inverters that can work at high switching frequencies. Using a

LC power filter will minimize the effects of the high switching frequency of the inverter on the motor but the filters are very expensive and inefficient, up to 50% of the inverter power is lost due to losses in the LC filter, some application such as vector control used in variable speed drives cannot work using inverter with output power filters.

The method for motor overvoltage suppression presented in this paper can be used in variable speed system with high power motors and long cables.

REFERENCES

1. J. Luszcz, K. Iwan, *Conducted EMI propagation in inverter-fed AC motors,* Electrical Power quality and Utilisation, Magazine Vol. II, No.1, 2006.

2. I.Tilea, C. Munteanu, *Study of electromagnetic interference in inverter driven asynchronous motors*, *World Energy System Conference,* 2012.

3. I.Tilea, C. Munteanu, *Overvoltage analysis in inverter driven induction motors,* International Conference and Exposition on Electrical land Power Engineering, pag.509-512, 2012.

4. F. Zare, *EMI in Modern AC Motor Drive Systems*, IEEE International Symposium on EMC, 2007.

5. S. Ogasawara, H. Akagi, *Analysis and reduction of EMI conducted by a PWM inverter-fed AC motor drive system having long power cables*, Okayama University Digital Information Repository, 2000.

6. N. Mutoh, T. Konuma, *A motor-terminal surge and induced EMI noise controlling method effective in EVs with the high density packaging structure*, Vehicle Power and Propulsion Conference, 2008. VPPC '08. IEEE, pag. 1-7.

7. S. Lee, K. Nam, *Overvoltage Suppression Filter Design Methods Based on Voltage Reflection Theory*, IEEE TRANSACTIONS ON POWER ELECTRONICS, VOL. 19, NO. 2, 2004.

8. O. Henze , H.D. Gersem, *Simulation of wave propagation phenmena in inverter-fed drives*, DFG Reasearch Group FOR575 , Anual report for 2005/2006.

THE STUDY OF TRANSIENT PROCESSES IN THE ASYNCHRONOUS STARTING OF THE SYNCHRONOUS MOTOR

Alexandru **BÎRLEA**, Olivian **CHIVER**
Eaton Electroproduction Romania, Technical University of Cluj-Napoca

Key words: Transient processes, synchronous motor, asynchronous starting

Abstract*: Starting synchronous motors can be achieved by several methods: starting with an auxiliary motor launch, starting in asynchronous regim, by feeding from a variable frequency source, auto-synchronization with the network.. In our case we study the transient processes in a asynchronous regim . In this case the synchronous motor is started like a squirrel cage induction motor . To start, the synchronous motor is equipped with a starting winding cage placed in the pole pieces of polar inducers; later , during the operation, this acts as a damping winding. Large synchronous motors have pole pieces made from massive polar inducers fulfilling the role of a cage winding*

1. INTRODUCTION

The synchronous motor develops an average synchronous torque only at synchronous angular speed operation $\Omega_1 = \omega_1 / p$. At a different speed as well as when starting, the synchronous motor connected to an AC mains and excited in DC develops a synchronous, alternating electromagnetic torque, its average value over a period of induced currents in the rotor being zero. At starting the induced currents' frequency is equal to the line frequency; the electromagnetic synchronous torque varies periodically with the same frequency. To turn the engine during a semiperiod requires that the moment of inertia and frequency should be low enough to permit the received energy from the stator to be sufficient to accelarate the rotor to its synchronous speed; in case of industrial frequency this is possible only in a microsynchronous motor.

2. THEORETICAL ASPECTS OF STARTING SYNCHRONOUS MOTORS

Starting synchronous motors can be achieved by several methods: starting with an auxiliary motor launch, starting in asynchronous regim, by feeding from a variable frequency source, auto-synchronization with the network.

In our case we study the transient processes in a asynchronous regim . In this case the synchronous motor is started like a squirrel cage induction motor . To start, the synchronous motor is equipped with a starting winding cage placed in the pole pieces of polar inducers; later , during the operation, this acts as a damping winding. Large synchronous motors have pole pieces made from massive polar inducers fulfilling the role of a cage winding.

Switching is done by connecting the motor directly to the network, or indirectly through a reactance of an autotransformer with two or more steps starting or star-delta method, based on admissible currents at startup and the load torque of the engine. During asynchronous starting the excitation winding is disconnected from the power supply of DC and the coil ends are connected across a rheostat with a resistance value of about 5 - 10 times higher than the excitation winding resistance . Excitation winding is not shorted at starting because a couple of uniaxial link can appear due to the single – phase induced in excitation winding, which would cause a saddle mechanical feature in starting a motor in asynchron.

Excitation winding is not left open because high voltage could be induced which could pierce its insulation.

Figure 1 shows the electromagnetic torque curve was plotted for the case where the excitation winding terminals are shorted (curve a) and connected to a resistance (curve b); in the latter case, mechanical characteristic saddle is lower and the danger of hanging the rotor at a speed approximately equal to (1/2) n1 is virtually eliminated.

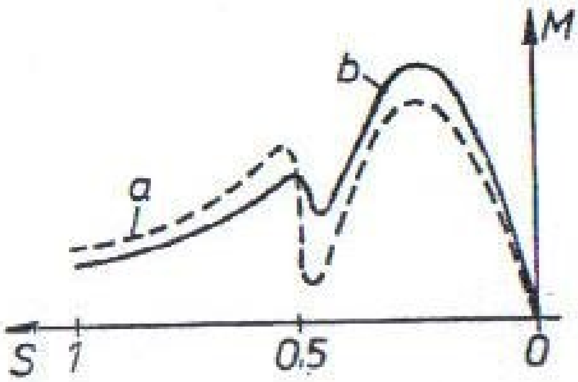

Fig. 1. Electromagnetic torque in synchronous operation
a - excitation winding connected in shorted method; b-excitation winding connected to a resistance

The unbalanced damping winding has a similar effect caused by the lack of the cross bars in the transverse axis and possibly, of the shorting ring segments from pole to pole. To partly dispose of these effects the damping winding bars are front short-circuited by complete rings.

After starting, the asynchronous motor speed is below synchronous speed, slip is less than 2 ... 3%, depending on the mechanical characteristic in asynchronous regim and the torque load. To synchronize the motor, disconnect the starting resistance of excitation winding terminals and connect the excitation source. The synchronous torque is produced by the interaction of the magnetic induction field produced by the rotor and the stator magnetic field, which is a rotating field to the rotor, with the rotor's sliding angular velocity in relation with the synchronous velocity; in the induction motor with poles growing out a synchronous torque reaction develops, which can produce, under certain conditions, the synchronization of the induction motor just before the rotor excitation.

In asynchronous regim, the steady, resistant torque is balanced by the asynchronous electromagnetic torque and the synchronous torque is zero; when operating in synchronism, the resistant torque is balanced by the synchronous torque and asynchronous torque is zero.

3. EXPERIMENTAL STUDY

For the experimental study of the synchronous motor starting asynchronously, the measurements were performed on a synchronous motor having the following characteristics: TYPE SCI 400, 1971, U = 400V, I = 7.2 A; 5KVA, cosφ 0.8; 3000rot/min; 50Hz IP23. For starting I used an automation made by contactors and timers, automation wiring diagram being shown in the figure below. Red dots indicate locations where we have made measurements with Fluke device 435.

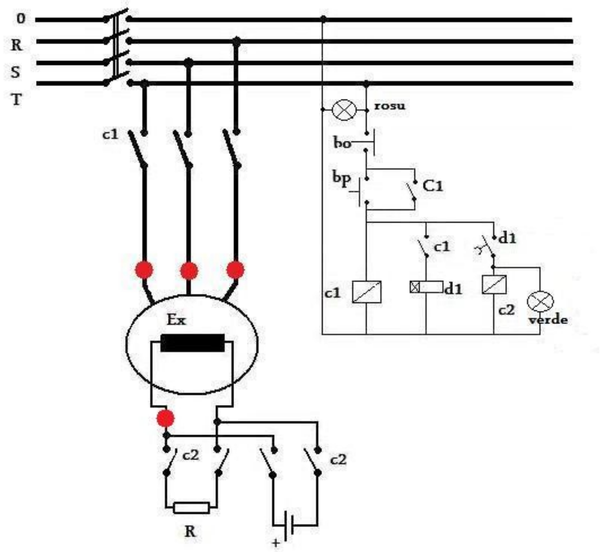

Fig 2 Automation scheme and points where measurements are taken.

To be able to see transients that occur in the transition from asynchronous to synchronous induction motor, Fluke 435 is set on inrush mode. Inrush currents are transient currents that occur when a high load is connected or at low impedance. Normally the current will stabilize after a while, when the load reaches normal operating conditions. For example, the starting current for the induction motor can be 10 times higher than the nominal operating current. Inrush mode is a "single shot" to register the voltage and current trend after the occurrence of an event (trigger). An event occurs when the current waveform exceeds settable limits.

Fig. 3 Fluke device for analyzing power

Several measurements have been made without mechanical loading of the synchronous motor, but we have varied the excitation voltage applied and the value of the resistance that has been connected to the ending wiring of the excitation coil.

Nr. Crt.	**Excitation voltage applied**	**Resistance value related to the excitation winding**	**Case**
1	10Vc.c.	90Ω	1
2	15Vc.c.	90Ω	2
3	20Vc.c.	90Ω	3
4	24Vc.c.	90Ω	4
5	30Vc.c.	90Ω	5
6	40Vc.c.	90Ω	6
7	10Vc.c.	190Ω	7
8	24Vc.c.	190Ω	8
9	40Vc.c.	190Ω	9

Case 1 **(10Vc.c., 90Ω):**

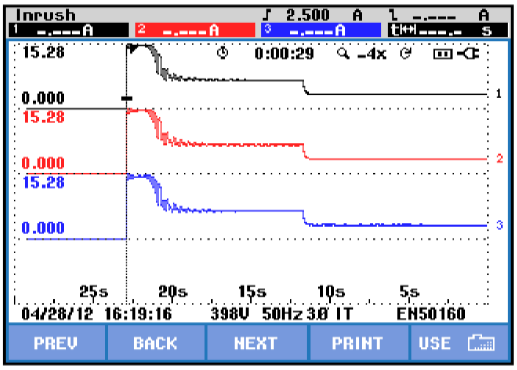

1.1

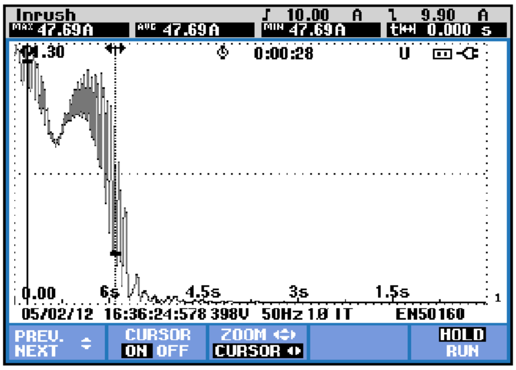

1.2

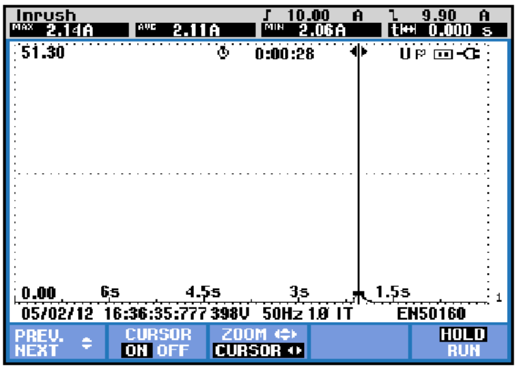

1.3

At 10Vc.c., applied voltage excitation, the synchronism entry is easy, without any current fluctuations, even with a decrease from the current asynchronous regim. Diagram 1.2 presents the the current variations and value (about 50A) when the synchronous motor is functioning in asynchronous regim. And in diagram 1.3, the entry into synchronicity is pointed out by a small leap of current (2 A).

Case 2 **(15Vc.c., 90Ω):**

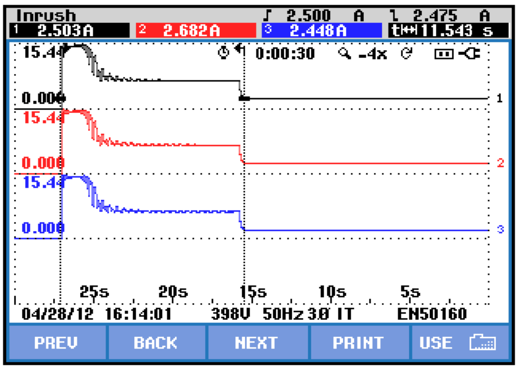

2.1

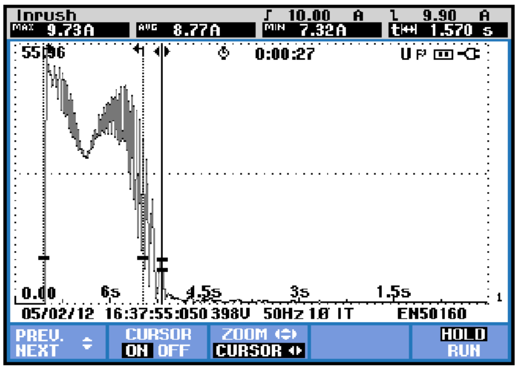

2.2

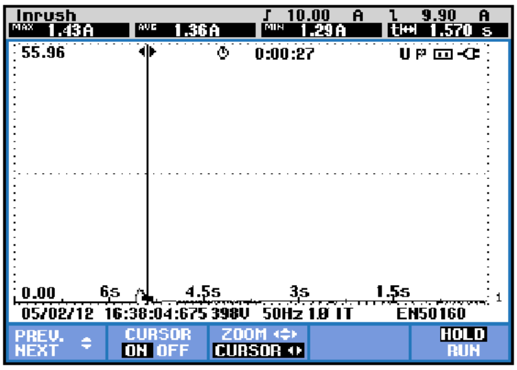

2.3

Figure 2.1 shows values and changes in the starting current wave absorbed by the motor, similar to the previous case, and Figure 2.2 presents the variation of current wave which is the same as in the previous case, only when entering in the synchronization, the current fluctuation has slightly increased.

***Case 3* (20Vc.c., 90Ω):**

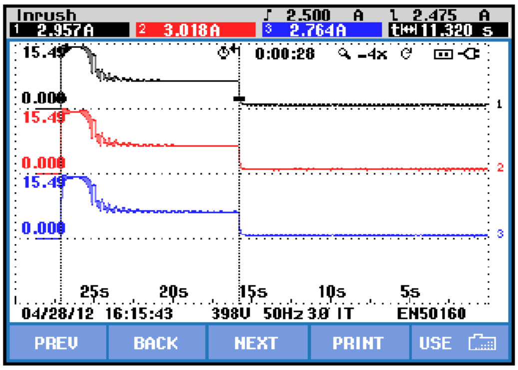

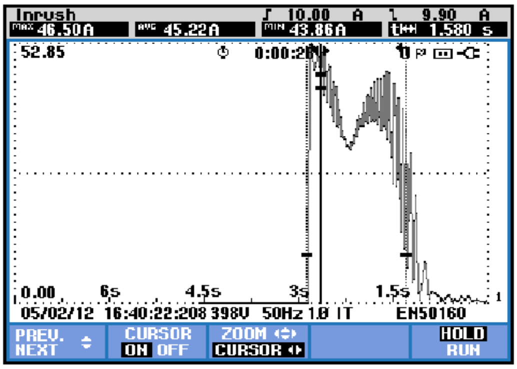

3.1 3.2

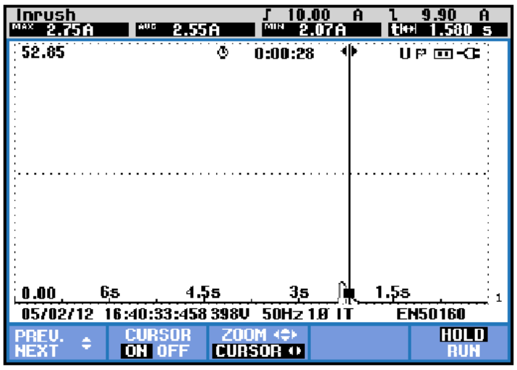

3.3

At 20V d.c. voltage applied to the excitation winding, the currents are similar to previous cases in both points of measurement.

Case 4 **(24Vc.c., 90Ω):**

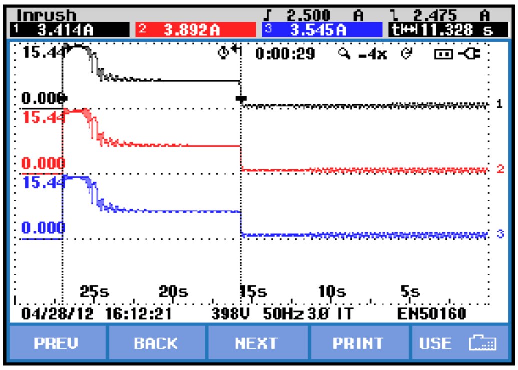

4.1

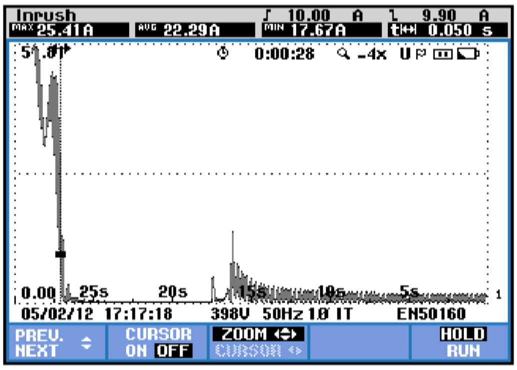

4.2

In this case the starting is the same as in the previous cases, except that after a while of running in synchronous regim, some fluctuations of curent occur which produce mechanical vibration. In figure 4.2. an aperiodic component appears at the entry into synchronicity which is amortized in time to a certain value.

Case 5 **(30Vc.c., 90Ω):**

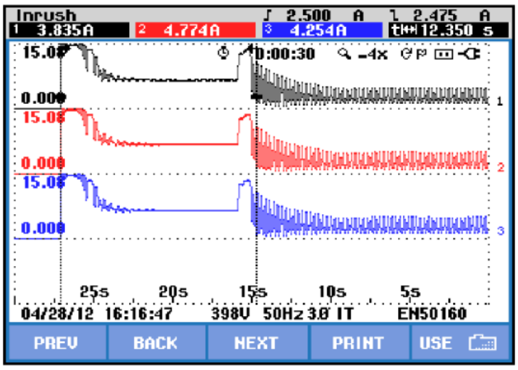

5.1

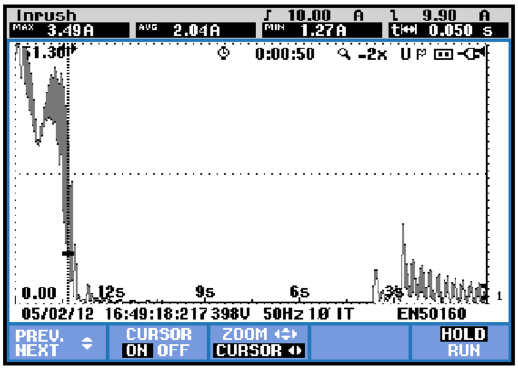

5.2

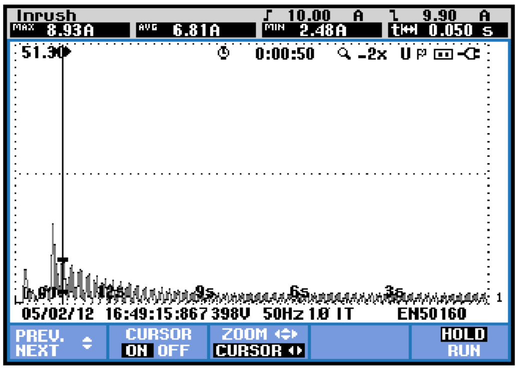

5.3

In this case, a current close to the starting current appears at synchronous entry, and continues with some intereferences and mechanical vibrations that no longer attenuate during running. On the excitation winding there is a jump of current at syncronicity entry followed by some current fluctuation that are no longer depreciated.

***Case 6* (40Vc.c., 90Ω):**

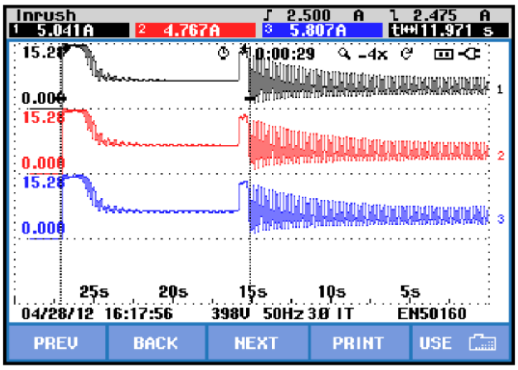

6.1

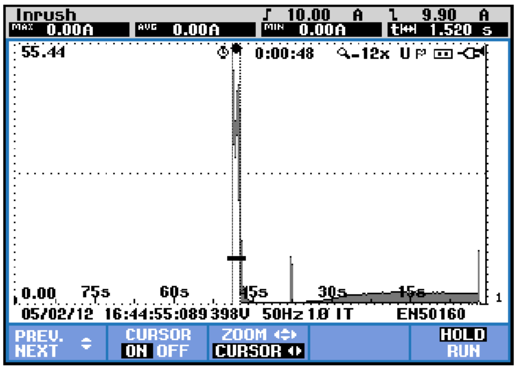

6.2

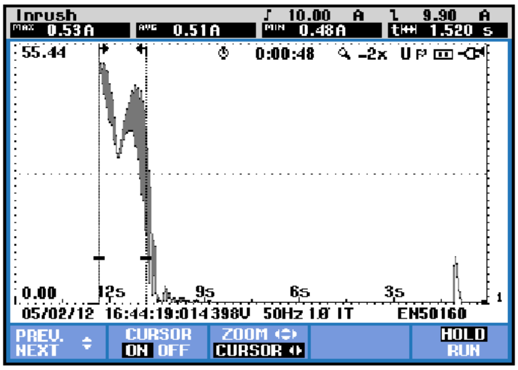

6.3

As in the previous case at synchronism entry the same current jump appears almost to the starting current, the running is continued with disturbances and mechanical vibrations that are no longer depreciated . Current fluctuations occur in the stator circuit (6.1) and the excitation winding (6.3).

***Case 7* (10Vc.c., 190Ω) :**

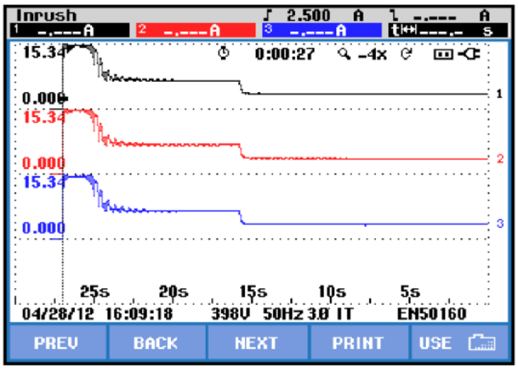

7.1

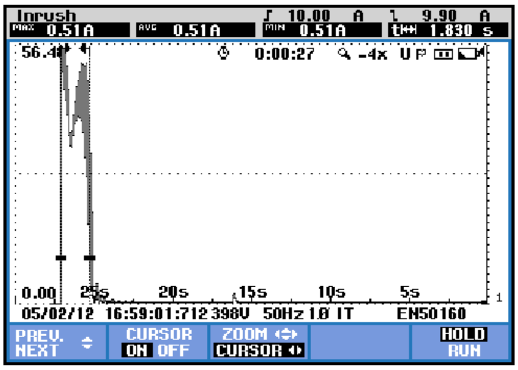

7.2

Current fluctuations and the waveform are the same as in case 1 where the resistance is half.

***Case 8* (24Vc.c., 190Ω):**

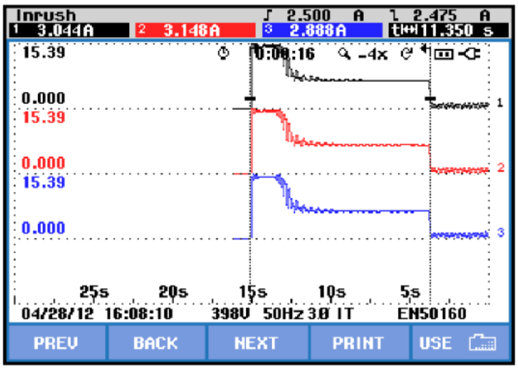

8.1

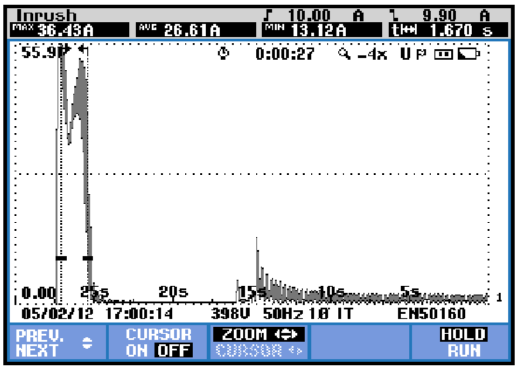

8.2

As in the previous case, when the resistance connected to the excitation winding has 90 Ω value, the starting current has the same value as the starting currents, even the disturbance and mechanical vibration are still present .

***Case 9* (40Vc.c., 190Ω):**

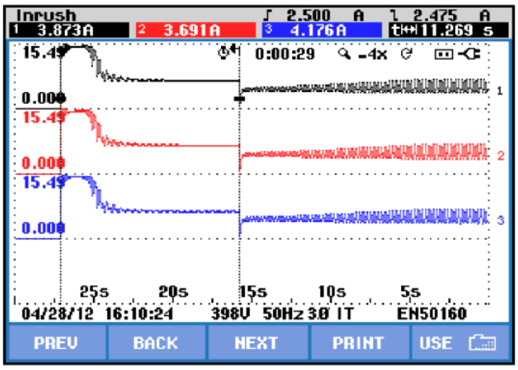

9.1

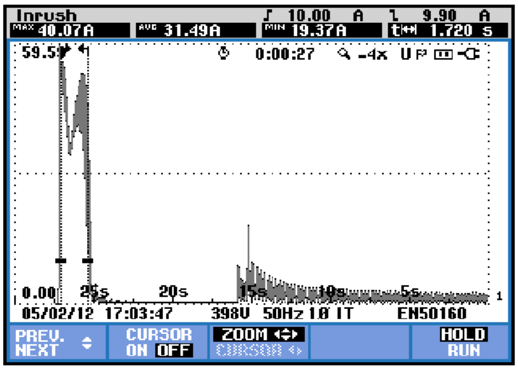

9.2

In this case, fig. 9.1. shows that at the entry into syncronicity there is a decrease of current value followed by some fluctuation in current that is amplified and remains present throught the whole period of engine operation, producing large mechanical vibration. In the rotor the *aperiodic* component is amortized up to a certain value.

Observation

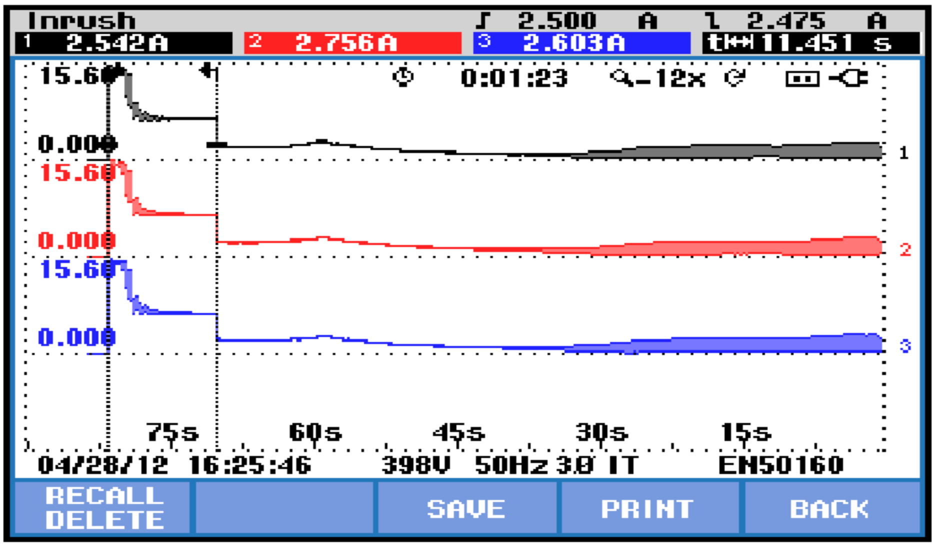

Without a mechanical loading at 20Vc.c., on the excitation winding of the synchronous motor terminals there can be found the lowest current of 0.8 A.

4. CONCLUSIONS

When starting a synchornous motor in asynchronous regim the current surge relies heavily on the starting cage, not on the resistance connected to the excitation winding . This only has an influence on the maximum current in the excitation winding. For a better synchonization, is appropriate to use such a voltage on the excitation winding, as to make sure the synchronization regim is an inductive one. In the studied case at a voltage of 10Vc.c. synchronization is very smooth. The excitation voltage at which the full load power factor is unit is worth about 24Vc.c.

REFERENCES

1. I. Novac, E. Micu, **ş.a**., *Machines and drives*, Editura Didactică şi Pedagogică, Bucureşti – 1982

2. Aurel Cîmpeanu, *Electric machines*, Scrisul românesc, Craiova, 1977

3. Aurel Cîmpeanu, Ion Vlad, *Electric machines*, Editura Universitaria, Craiova, 2008

4. Fluke 435 User guide

5. Aurel Câmpeanu, Ion Vlad, *Complements of dynamic electric cars*, Editura Universitaria Craiova, 2007

THE ROUTH AND HURWITZ STABILITY STUDY USING LABVIEW PROGRAMME

Barz **CRISTIAN**, Oprea **CONSTANTIN**
Technical University of Cluj-Napoca, North University Center from Baia Mare
cristian.barz@ubm.ro, prconstantin@yahoo.com

Key words: automatic systems stability, LabVIEW platform

Abstract*: Because the automatic system stability analytic study is very difficult to achieve, the paper presents some computer programmers realized in "LabVIEW" and useful for the study. The programmers were done taking into account the stability of the systems [1, 2, 3, 4] without insisting too much on the theoretical problems.*

1. THEORETICAL CONSIDERATIONS

The problem of the linear and nonlinear automatic systems stability is very complex because in the case of systems with negative reaction, there is the possibility, in certain circumstances to get out of control. This state is actually instability because the signals transmitted and processed in the system are no longer the result of the commands given. The stability of a system is first required as a designing condition and secondly as an operation condition because in many cases a simple wanted or not wanted variation of a constructive parameter can cause the system's instability. The systems that are stabile only for certain constructive parameters values are known as conditioned stable systems.

Can be declared that an automatic system is stable if, after a given command or a disturbance the emergence signal e(t) tend to a stationary value and the weight function y(t) tends to zero:

$$\lim_{t \to \infty} e(t) = e_{st.}; \lim_{t \to \infty} y(t) = 0 \tag{1}$$

the condition required for the weight function being more general because it does not suppose the existence of a command signal.

Considering a close circuit system with: Yd(s) – transfer function on the direct curl, Yr(s) – transfer function on the reaction curl, s = jω (j = $\sqrt{-1}$; ω – pulsation), the system's function is:

$$Y_o(s) = \frac{Y_d(s)}{1 + Y_d(s) \cdot Y_r(s)} \tag{2}$$

The problem of the described (2) system's stability occurs when analyzing the poles of this function, which means the zeroes of the polinom:

$$1 + Y_d(s) \cdot Y_r(s) = 0 \tag{3}$$

more precisely the existence or inexistence of positive zeroes or complex conjugated with positive real part zeroes.

To solve the stability systems problem were realized many stability criterions such as: Routh and Hurwitz; Liapunov; Lienard-Chipard; Bode (in logarithmic diagrams); etc.

The analytic solution for this stability study using these criterions is very laborious. That's why in this paper is offered a solution by expanding "LabVIEW" programmer area.

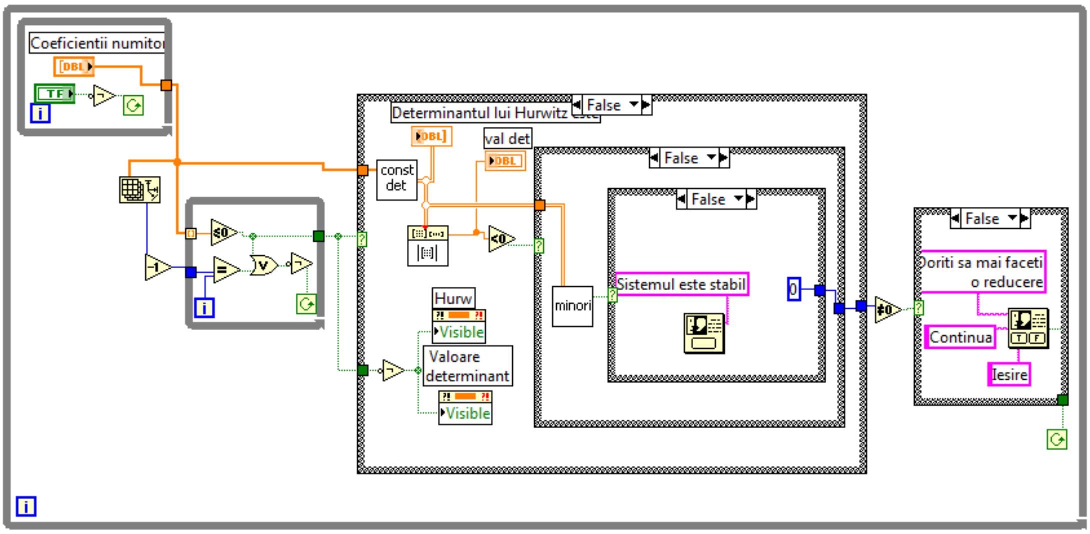

Fig 1.1. Routh – Hurwitz stability criterion (algebraically)

Even if many papers present them separately, both have the same essence, being algebraic criterions that analyses the stable asymptotic character of a system by determining the inexistence of positive real part of the characteristic polinomous (3), but without actually finding these roots.

We are considering an autonom linear system with the following matrices' equation:

$$\mathbf{x}^{\mathrm{T}}(t) = \mathbf{A}^*\mathbf{x}(t) \qquad \text{t (4)}$$

where $\mathbf{x}^{\mathrm{T}} = (x_1, x_2, \ldots x_n)$ – state vector; A – coefficients matrices, constant, nonsingular and with definite (n*m) elements. The system described by such an equation is asymptotic stable, if and only if all the values belonging to A are at the same time the roots of the characteristic polinom:

$$det\,[s\mathbf{I} - \mathbf{A}] = a_{0^*}s^n + a_{1^*}s^{n-1} + \ldots\ldots a_{n-1^*}s + a_n \tag{5}$$

where s = d/dt is the derivation operator and **I** is the unit matrices.

The polinom who's roots are negative or with negative real part is known as *Hurwitz polinom*.

Results that, if the characteristic polinom of the analyses system is a Hurwitz polinom the studied system is asymptotic stable.

One of the conditions required, but not sufficient for a polinom to be Hurwitz polinom is all the coefficients to be positive and different from zero:

$$a_1/a_0 > 0;\ a_2/a_0 > 0;\ \ldots\ldots a_n/a_0 > 0 \qquad (6)$$

$$\left|\begin{array}{lllll} a_0 & a_2 & a_4 \ldots\ldots a_{n-2} & a_n \\ a_1 & a_3 & a_5 \ldots\ldots 0 & 0 \\ b_1 & b_2 & b_3 \ldots\ldots 0 & 0 \\ c_1 & c_2 & c_3 \ldots\ldots 0 & 0 \\ \ldots\ldots & \ldots\ldots & \ldots\ldots & \ldots \\ d_1 & d_2 & 0 \ldots\ldots 0 & 0 \\ e_1 & e_2 & 0 \ldots\ldots 0 & 0 \\ f_1 & 0 & 0 \ldots\ldots 0 & 0 \\ g_1 & 0 & 0 \ldots\ldots 0 & 0 \end{array}\right| \qquad (7)$$

condition that can be verified immediately [3].

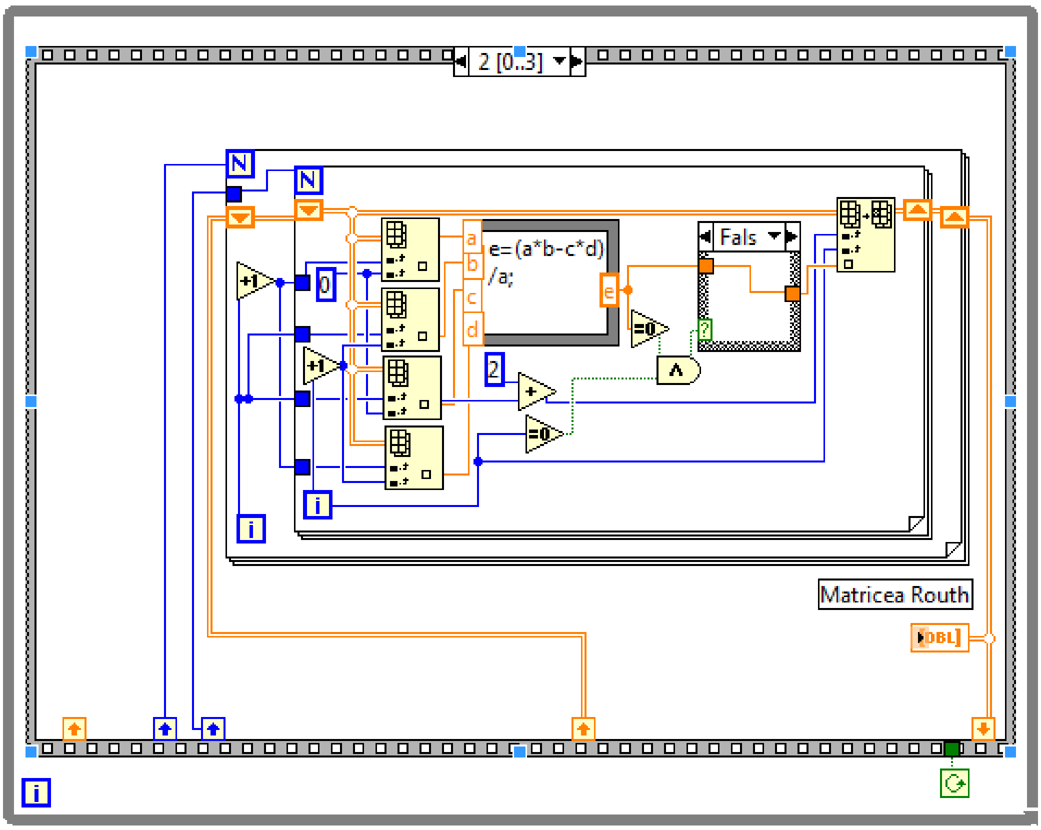

Fig 1.2. The Routh matrice

In Routh's formulation, using the polinom coefficients [5] is obtained the following table:
where the first two lines are formed by the polinom coefficients (5), the followings are calculated with the expressions:

$$b_1 = \frac{a_1 \cdot a_2 - a_0 \cdot a_3}{a_1}; b_2 = \frac{a_1 \cdot a_4 - a_0 \cdot a_3}{a_1}; b_3 = \frac{a_1 \cdot a_6 - a_0 \cdot a_7}{a_1} \ldots.$$
$$c_1 = \frac{b_1 \cdot a_3 - b_2 \cdot a_1}{b_1}; c_2 = \frac{b_1 \cdot a_5 - b_3 \cdot a_1}{b_1}; c_3 = \frac{b_1 \cdot a_7 - b_4 \cdot a_1}{b_1} \ldots. \quad (8)$$

and the last two lines are:

$$f_1 = \frac{e_1 \cdot d_2 - d_1 \cdot e_2}{e_1}; \quad g_1 = e_2 \quad (9)$$

Totally will be n+1 lines, two successive lines having the same numbers of terms different from zero, excepting the second line which can have a term less than the first one, in case that the polinom degree is odd (the presented case).

The polinom (5) is a Hurwitz polinom and results that the system characterized by it is asymptotic stable if the inequalities (6) are fulfilled and also all the terms of the first column in (7) are positive:

$$a_0 > 0; a_1 > 0; b_1 > 0; \ldots\ldots f_1 > 0; g_1 > 0 \quad (10)$$

In case condition (10) is not fulfilled, results that the polinom (5) is not a Hurwitz polinom, the table (7) showing us the number of the positive roots or the roots with positive real part of the polinom, number equal with the number of the sign changes that appear in the first column of the table.

2. CONCLUSIONS

Depending on the stability criterion suitable were realized programmers in "Lab VIEW"[5,6] and based on concrete systems examples with analytic verified stability the programmers were used. The results obtained were very good, the advantage of using these programmers being the work time that can be considered infinitesimal compared with the time necessary for analytic solving and the work accuracy that can't be expressed. With the mention that the programmers were made for the stability criterions: Routh-Hurwitz; Lienard-Chipard; Liapunov; Nyquist; Bode(in logarithmic diagrams that can be success-fully also used for automatic not linear systems based on the description function), the theoretic aspect of the other criterions are not presented in the paper. Are recommended [1,2,3,4].

REFERENCES

1. Hăngănuţ M., *Automatică,* Editura Didactică şi Pedagogică, Bucureşti, 1971.

2. Hăngănuţ M., Dancea I., Negru O., *Programe FORTRAN comentate în automatică,* Editura Tehnică, Bucureşti, 1974.

3. Oprea C., *Automatică,* Editura Risoprint, Cluj Napoca, 2000.

4. Oprea, C., Barz, Cr., *Elemente de inginerie electrica, reglare automata si automatizari,* Risoprint, Cluj Napoca, 2011.

5. *** *LabVIEW, User Manual,* Natonal Instrument, USA, 2010.

6. *** *LabVIEW, Programming, Reference Manual,* Natonal Instrument, USA, 2010.

INSTRUCTIONS FOR AUTHORS

Name **SURNAME**, Name **SURNAME, ...**
Affiliation, email of 1st author, Affiliation, email of 2nd author, ...

Key words: List 3-4 keywords
Abstract: *Abstract of max. 120 words*

1. INTRODUCTION

The paper must be written in English. It shall contain at least the following chapters: Introduction, research course (mathematical algorithm); method used; results and conclusions, references.

Use DIN A4 Format (297 x 210 mm) MSWord format. Margins: top, bottom, left and right 2.5 mm each. The text should be written on one side of the page only. Use Times New Roman fonts, line spacing 1.3. The font formats are: paper title: 14 pt bold italic, capital letters, author's name(s): 12 pt italic for name and 12 pt. bold, italic for surname; Affiliation: 11 pt. italic; key words: 10 pt, bold; Abstract: 10 pt. italic, word Abstract in 10 pt. bold; chapter titles (do not use automatic numbering): 12 pt bold, capital letters; subtitles: 12 pt bold lower capitals; body text: 12 pt. regular. tables and figures caption: 11 pt. italic; references: author 11 pt. bold, title 11 pt. italic, year, pages, ... in regular.

The number of pages is not restricted.

2. FIGURES AND TABLES

Figures have to be made in high quality, which is suitable for reproduction and print. Don't include photos or color prints. Place figures and tables at the top or bottom of a page wherever possible, as close as possible to the first reference to them in the paper.

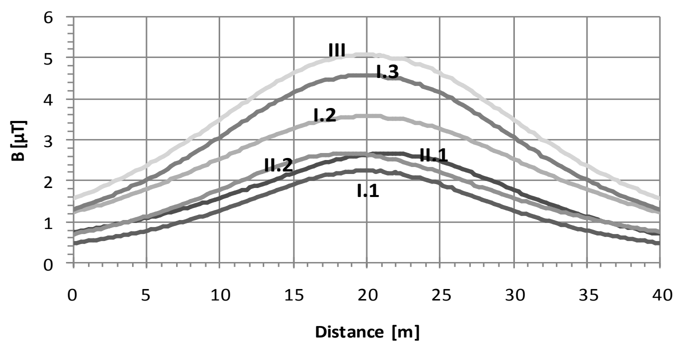

Fig. 4 - Magnetic flux density at 1 m above the ground

Table1. Transposing principle

	Circuit											
	1	*2*	*1*	*2*	*1*	*2*	*1*	*2*	*1*	*2*	***1***	***2***
1/3	*R*	*T*	***R***	***R***	*R*	*S*	*R*	*T*	*R*	*S*	***R***	***R***
line	***S***	***S***	*S*	*T*	*S*	*R*	*S*	*R*	*S*	*T*	***S***	***S***
length	*T*	*R*	*T*	*S*	***T***	***T***	*T*	*S*	*T*	*R*	***T***	***T***
1/3	*T*	*S*	***T***	***T***	*T*	*R*	*T*	*S*	*T*	*R*	***T***	***T***
line	***R***	***R***	*R*	*S*	*R*	*T*	*R*	*T*	*R*	*S*	***R***	***R***
length	*S*	*T*	*S*	*R*	***S***	***S***	*S*	*R*	*S*	*T*	***S***	***S***
1/3	*S*	*R*	***S***	***S***	*S*	*T*	*S*	*R*	*S*	*T*	***S***	***S***
line	***T***	***T***	*T*	*S*	*T*	*S*	*T*	*S*	*T*	*R*	***T***	***T***
length	*R*	*S*	*R*	*T*	***R***	***R***	*R*	*T*	*R*	*S*	***R***	***R***
Name	***I.1***		***I.2***		***I.3***		***II.1***		***II.2***		***III***	

3. EQUATIONS

Equations are centred on page and are numbered in round parentheses, flush to right margin. In text respect the following rules: all variables are italic, constants are regular; the references are cited in the text between right parentheses: [1], the list of references has to be arranged in order of citation.

REFERENCES

1. International Commission on Non-ionizing Radiation Protection, *Guidelines for limiting exposure to time-varying electric, magnetic and electromagnetic fields (Up to 300 GHz)*, Health Physics, **74**, pp. 494-522, 1998.

2. A. Marincu, M. Greconici, *The electromagnetic field around a high voltage 110 KV electrical overhead lines and the influence on the biological sistems,* Proceedings of the 5th International Power Systems Conference, pp. 357-362, Timisoara, 2003.

3. Gh. Hortopan, *Compatibilitate electromagnetică,* Ed. Tehnică, 2005.